Atmospheric Research 320 (2025) 108068

Contents lists available at ScienceDirect

Atmospheric Research

journal homepage: www.elsevier.com/locate/atmosres

Influence of local topographic structures on the atmospheric mechanisms related to the Andean-Amazon rainiest zone

Ricardo A. Gutierrez-Villarreal [a,b,*], Clémentine Junquas [c,d], Jhan-Carlo Espinoza [c,e], Patrice Baby [f], Elisa Armijos [a,b]

[a] Escuela de Posgrado, Universidad Nacional Agraria La Molina, Lima, Peru
[b] Subdirección de Ciencias de la Atmósfera e Hidrósfera, Instituto Geofísico del Perú, Lima, Peru
[c] Univ. Grenoble Alpes, IRD, CNRS, INRAE, Grenoble-INP, IGE, 38000 Grenoble, France
[d] Servicio Nacional de Meteorología e Hidrología, Lima, Peru
[e] Instituto de Investigación sobre la Enseñanza de las Matemáticas, Pontificia Universidad Católica del Perú, Lima 15088, Peru
[f] Géosciences Environnement Toulouse, Université Paul Sabatier, IRD, CNRS, 31400 Toulouse, France

ARTICLE INFO

Keywords:
Precipitation hotspots
Andes-Amazon transition region
WRF model
Topography
Sensitivity experiments
Peru

ABSTRACT

The Andes-Amazon transition region features critically important ecological services on the local, regional and global scales. This region is among the rainiest zones in the world, with rainfall rates of up to 7000 mm/year. However, the physical mechanisms leading to the existence of these "precipitation hotspots" remain poorly known. Here, we attempt to disentangle the controlling atmospheric mechanisms exerted by local topographic structures that started to uplift about 5–10 million years ago in response to the Nazca Ridge subduction, in the vicinity of the Quincemil hotspot, the most intense of them. We first use the Weather Research and Forecasting model to conduct sensitivity tests to planetary boundary layer parameterizations at 5 km horizontal grid spacing during the austral summer of 2012–13. After finding the most suitable configuration in terms of the diurnal cycle of rainfall intensity and extent, we further perform topographic sensitivity tests by reducing the Fitzcarrald Arch lowlands and, on top of it, by removing the Camisea mountain. The Fitzcarrald Arch deflects moisture flux towards Quincemil, while the Camisea mountain induces local vortical circulations that increase moisture transport, convergence and rainfall over Quincemil, ultimately controlling its location and intensity by up to 40 %. When reducing the height of the Andes in half, we find that it sustains the development of precipitation hotspots, accounting for up to 60 % of rainfall, by providing a mechanical forcing to increase regional-scale moisture fluxes. Such mechanisms dominate during nighttime, when rainfall peaks in the region, and might explain the existence of the rainiest zone in the Andes-Amazon transition.

1. Introduction

The Andes-Amazon transition region, situated at the eastern flank of the Andean cordillera, is the rainiest and most biodiverse area within the Amazon basin (Espinoza et al., 2015; Hoorn et al., 2010). The development of this biodiversity is believed to be driven by interactions between plate tectonics, land surface dynamics and atmospheric circulation (Antonelli et al., 2018; Hoorn et al., 2010). These processes are mainly controlled by the uplift of the Andes over the last 65 million years and are fundamental to the evolution of Amazonian ecosystems and landscapes (Sacek et al., 2023), enabling new species to develop (Hoorn et al., 2010; Roncal et al., 2015). In addition, rainfall over the Andes-Amazon transition region strongly modulates sediment transport at the basin scale in Amazonia (Armijos et al., 2020), which is a key process for sustaining the extraordinary biodiversity in this basin (Beveridge et al., 2024).

Particularly, about 5–10 million years ago, a topographic feature known as the Fitzcarrald Arch started to uplift due to the subduction of the Nazca Ridge beneath the South American Plate (Espurt et al., 2007, 2009; Regard et al., 2009). This structure, which does not exceed the height of 600 m.a.s.l., is located in the Andean-Amazonian retro-foreland basin of southern Peru (Fig. 1), at the vicinity of the rainiest region of the Andean foothills, known as the Quincemil hotspot (Chavez and Takahashi, 2017; Espinoza et al., 2015). This period coincides with the

* Corresponding author.
E-mail address: 20221639@lamolina.edu.pe (R.A. Gutierrez-Villarreal).

https://doi.org/10.1016/j.atmosres.2025.108068
Received 10 July 2024; Received in revised form 8 March 2025; Accepted 13 March 2025
Available online 16 March 2025

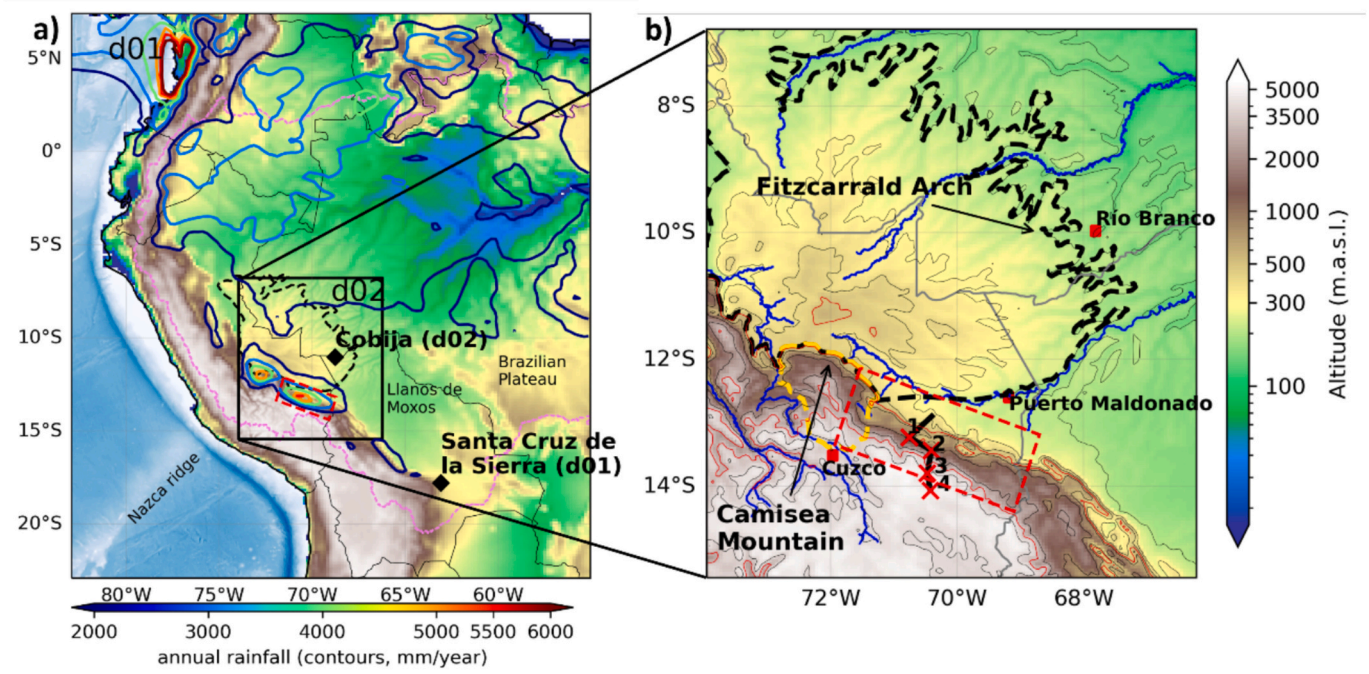

Fig. 1. a) Domains of the WRF simulations. Black diamonds represent the locations of sites used to construct vertical profiles of winds: Santa Cruz de la Sierra in d01 and Cobija in d02. The dashed violet line bounds the Amazon basin, and selected contour values (see the colorbar) represent annual rainfall over the domain area based on a climatology (2000–2020) of CMORPH estimates The Fitzcarrald Arch is bounded by the dashed black line. The location of secondary regions such as the Llanos de Moxos and the Brazilian Plateau is shown in thin black characters. The dotted red rectangles in both a) and b) represent an approximate location of the Quincemil hotspot. Sea bathymetry data was obtained from the General Bathymetric Chart of the Oceans (https://www.gebco.net). The Nazca ridge is oriented from the southwest to the northeast. b) Geographical details of the Amazon-Andes transition region around the Fitzcarrald Arch and Quincemil hotspot. The Fitzcarrald Arch is bounded by the dashed black line, while the dashed golden line represents the Camisea mountain. Main rivers are delineated by blue lines. Red squares and crosses represent the locations of major cities and rain-gauge records used in this study. Weather stations names are represented by numbers: 1 is Quincemil, 2 is San Gabán, 3 is Macusaní, 4 is Ollachea. Thick black lines delineate the path followed to construct precipitation/altitude transects. The thin red lines represent the 500 and 3000 m.a.s.l., while the thin black lines represent the altitudes of 50, 100, 150, 200, 300, 400, 600, 1000, 2000 and 4000 m.a.s.l.. (For interpretation of the references to color in this figure legend, the reader is referred to the web version of this article.)

apparition of new species of flora and fauna around the Fitzcarrald Arch (e.g., Athaydes et al., 2021; Roncal et al., 2015), a region also known for the abundance of Miocene fossils remains (Tejada-Lara et al., 2015). Thus, a better understanding of the links between climate and topography is needed to comprehend the processes that shaped the biodiversity richness in this region.

The climate of the Andes-Amazon transition region is the result of the interplay between large-scale and local-scale atmospheric circulation patterns, and the complexities of its physio-geographical features (Espinoza et al., 2020). Precipitation occurs all year long, but is more intense during the austral summer (DJF), in association with the mature phase of the South American Monsoon System (SAMS, Vera et al., 2006a). As prevailing winds transport moisture from the Atlantic Ocean and the Amazon basin towards the core of the SAMS, it forms a conduit of high-speed moist wind along the eastern flank of the Andes, known as the South American Low Level Jet (SALLJ; Marengo et al., 2004; Vera et al., 2006b). SALLJ-associated moisture transport towards the Andes-Amazon transition peaks during the summer (Li and Le Treut, 1999; Marengo et al., 2004) and, due to orographic blocking, it sustains the existence of rainfall hotspots along the exposed flank (Garreaud, 2009; Junquas et al., 2018; Romatschke and Houze, 2010).

The atmospheric processes associated with the diurnal cycle of rainfall at the local scale are controlled by thermally and mechanically forced circulations, both associated with local topography (Garreaud, 1999; Junquas et al., 2018, 2022; Trachte et al., 2010). During daytime, the radiative warming of the surface induces thermally-driven anabatic (upslope) winds in valleys and slopes, transporting moisture and favoring convection over mountain summits. This mechanism explains the daytime precipitation maximum found over several Andean top valleys (Flores-Rojas et al., 2021; Junquas et al., 2018, 2022; Rosales et al., 2022). In the hotspot region, this surface upslope process weakens the mechanical blocking process of the Amazon regional moisture flux over the Andes, leading to a weakening of the hotspot convection and precipitation during daytime. However, during the nighttime, the radiative cooling of the surface induces katabatic (downslope) winds from the summits, which are particularly important over the eastern flank of the tropical Andes (Junquas et al., 2018, 2022; Trachte et al., 2010). Still during the nighttime, the regional-scale SALLJ-associated moisture flux from the Amazon lowlands is accelerated which is consistent with decreases in eddy viscosity due to the planetary boundary layer (PBL) stabilization (Blackadar, 1957). The convergence of both nighttime katabatic winds and SALLJ-associated moisture flux explains the nocturnal precipitation maximum found over the eastern flank of the Andes and, particularly, the Quincemil hotspot (Chavez and Takahashi, 2017; Junquas et al., 2018). This interaction of local-to-regional scales results in about 70 % of summertime rainfall at the eastern Andes foothills (including the Quincemil hotspot) being produced during the night (Chavez and Takahashi, 2017).

For the Andean cordillera, previous research based on climate simulations showed that the Andean cordillera as a whole exerts a significant influence in the lower tropospheric circulation due to mechanical forcing (Insel et al., 2010; Junquas et al., 2016; Saurral et al., 2015). These controls are less significant in the upper tropospheric circulation, as it is mainly a response to latent heat release by the summer convection over the Amazon basin (Figueroa et al., 1995; Lenters and Cook, 1997). When the Andes are removed in numerical experiments, SALLJ-associated moisture transport is greatly weakened over the eastern flank of the Andes, suppressing convection along the rainfall hotspots (Insel

et al., 2010; Junquas et al., 2016; Poulsen et al., 2010; Saurral et al., 2015; Sepulchre et al., 2009). However, these previous investigations were conducted at the regional scale with grid spacings ranging from 2° to 0.6°. The fine details of spatio-temporal distribution of precipitation hotspots (e.g. Quincemil) and how they are affected by Andean heights at the local scale could not be examined.

Previous studies have demonstrated the necessity of high-resolution atmospheric models in order to resolve the mechanisms associated to rainfall at the topographically-complex Eastern Andes flanks (Junquas et al., 2018, 2024; Martinez et al., 2024; Trachte et al., 2009, 2010). In particular, for the Quincemil hotspot, Junquas et al. (2018) showed that high resolution modeling is useful in order to identify both synoptic and local mechanisms such as thermal-driven and mechanically-forced circulations in this region. Recently, Gutierrez et al. (2024) identified high-resolution models at 0.2° as better reproducing the location and intensity of the Quincemil hotspot, among a set of regional climate models from 0.2° to 0.5°. Therefore, recent improvements made in kilometer-scale atmospheric modeling could help in identifying the crucial role of topography over the hotspot of precipitation.

At local scales, the influence of several topographic structures in regional and local atmospheric mechanisms has been studied through experiments in high-resolution regional climate models ($\Delta x < 5$ km). Xiang et al. (2024) showed that the Hengduan Mountains, which is also a biodiversity hotspot and is located at the southwestern Tibetan plateau, serves as a local topographic barrier to large-scale moisture fluxes, which results in pronounced orographic precipitation in its vicinity. Junquas et al. (2018) and Gomez-Rios et al. (2023) illustrated the role of Andean valleys (Apurímac and Magdalena, respectively) in the channelization of moisture, which feeds convective processes downwind. Another Andean-associated topographic feature studied is the Córdoba ranges east of the Andes in Argentina for case studies of Mesoscale Convective Systems (MCS) (Mulholland et al., 2019; Rasmussen and Houze, 2016). They found that the Córdoba ranges focus convective initiation and results in more intense storms due to changes in internal MCS dynamics and environmental changes such as vertical wind shear and atmospheric instability. However, to our knowledge, no one has studied yet the impacts of local topography on the atmospheric processes leading to rainfall in the Quincemil hotspot, the rainiest zone in the Amazon basin.

In this study, we aim to elucidate the controls of local topographic structures on the atmospheric processes associated with the Quincemil hotspot. We do so by employing the Weather Research and Forecasting model (Skamarock et al., 2021) to simulate atmospheric conditions during DJF 2012–13 with both "control" (CTRL) conditions and modified topographies in a nested domain approach. The CTRL conditions are obtained by validating the model after a sensitivity test to three planetary boundary layer parameterizations. Next, in the topographic experiments performed, we eliminate the Fitzcarrald Arch, and an associated localized relief (the Camisea mountain) and reduce the height of the Andes; all of which are approximations to past states of local and regional topography.

2. Datasets and model

2.1. Precipitation data

To validate the model simulations in the Quincemil hotspots, we use precipitation data from 4 in-situ pluviometers operated by the National Service of Meteorology and Hydrology of Peru (see the red crosses in Fig. 1b). These gauges provide data every 12 h, at 07 and 19 LT (GMT −5:00) during December–February (DJF) of 2012–13 (with the exception of the Quincemil station during December 2012). This period was selected as it was close to the long-term average precipitation in the tropical Andes (e.g., Mourre et al., 2016). Due to the low density of in-situ precipitation records in the study area, we also consider series of precipitation gridded datasets with sub-daily temporal resolutions as references (Table 1). In addition, because the in-situ precipitation measurements are registered every 12 h, precipitation from the gridded datasets is averaged every 12 h (daytime: 07–19 LT, and nighttime: 19–07 LT). We use precipitation data from the TRMM's Precipitation Radar (TRMM-PR, version 7, product 2A25), which is subsequently referred to as "TRMM-2A25". The climatological product from DJF 2000–2014 is used, and was constructed by remapping the swath information into a Cartesian grid with pixels of 0.05° x 0.05° (see Chavez and Takahashi, 2017; and Junquas et al., 2018). We also use precipitation estimations of DJF 2012–13 from the CMORPH product (Joyce et al., 2004), with a grid size of ~8 km × 8 km. We also use a climatology (2015–2020) from the PISCOp_h product, which is a recent high-resolution gridded hourly precipitation developed by the National Service of Meteorology and Hydrology of Peru (Huerta et al., 2022). In order to keep the spatial consistency and signal of the satellite estimations, we use the non-diurnal-bias-corrected version, which we refer to as "PISCOph nonDBC" hereinafter. The quantitative biases of CMORPH and TRMM-2A25 have been addressed in previous studies (e.g., Espinoza et al., 2015; Huerta et al., 2022; Zubieta et al., 2019).

Table 1
Characteristics of the selected precipitation gridded datasets.

Gridded dataset	Selected time-window	Grid size	Original time frequency	Reference
TRMM PR version 7, producto 2A25	DJF 2000–2014 (climatology)	0.05° × 0.05°	One hour	TRMM Precipitation Radar Team (2011)
CMORPH	DJF 2012–13 (as the simulations)	8 km × 8 km	30 min	Joyce et al. (2004)
PISCOp_h non-diurnal-bias-corrected	DJF 2015–2020 (climatology)	0.1° × 0.1°	One hour	Huerta et al. (2022)

The climatological products TRMM-2A25 and PISCOph nonDBC are used qualitatively in this paper as a reference for characterizing the spatial distribution of precipitation and the intensity of the Quincemil hotspot during daytime and nighttime. The PISCOph nonDBC dataset does not have data before 2015. We could not use TRMM-2A25 specifically for the DJF 2012–13 period as it provides a low number of precipitation observations in the Andes for each hour in the day. For this reason, we averaged the product every 12 h and considered a 12-hourly climatology (2000–2014) in order to reduce uncertainties, as originally suggested by Negri et al. (2002). Note that shorter aggregations (e.g., 3 h) were used in previous studies (Junquas et al., 2018), but we decided to coarsen it to match the in-situ pluviometers' temporal frequency. Nevertheless, it can be regarded as a valid climatological product over the Quincemil hotspot (Espinoza et al., 2015; Junquas et al., 2018).

2.2. WRF model simulations

The WRF model version 4.3 (Skamarock et al., 2021) is used to simulate the atmospheric regional climate, including precipitation and atmospheric variables for DJF 2012–13. We select this period as it features low sea surface temperature anomalies in the Atlantic and Pacific

Table 2
Model setup characteristics at the two simulations domains.

	d01	d02
Forcing	ERA5	d01
Horizontal resolution	15 km	5 km
Nx	180	171
Ny	200	150
Nz	50	50
dt	75 s	25 s

Table 3
List of WRF physical parameterizations used in the simulations and the tested PBL schemes.

	Chosen/tested schemes	References
Microphysics	Morrison	Morrison et al. (2009)
Tested Planetary Boundary Layer parameterizations	ACM2	Pleim (2007)
	MYNN2.5	Nakanishi and Niino (2009)
	YSU	Hong et al. (2006)
Cumulus	New Tiedtke	Zhang and Wang (2017)
Land Surface	Noah-MP	Yang et al. (2011)
Surface layer	MM5 revised	Paulson (1970)
Longwave radiation	RRTM	Mlawer et al. (1997)
Shortwave radiation	Dudhia	Dudhia (1989)

Oceans, thus selecting a "normal" summer by limiting the effect of remote teleconnections. In addition, this period was also used in a 1-year WRF model assessment in the tropical Andes as it is close to 1965–2014 climatology (Mourre et al., 2016). The simulations begin in November 2012, with the first month being discarded as a spin-up. The model is non-hydrostatic and uses terrain-following vertical coordinates (sigma). The WRF model domains are setup as shown in Fig. 1 and Table 2, with a first domain (d01) set in tropical South America at 15 km resolution and forced by the ERA5 reanalysis (Hersbach et al., 2020), which has a spatial resolution of ~27 km. The second domain (d02) is centered in the Quincemil hotspot (Fig. 1b) with a resolution of 5 km. All domains use 50 vertical levels and the top of the atmosphere is set at 50 hPa. The selected physical parameterization schemes are listed in Table 3. We first perform three sensitivity experiments to PBL parameterizations.

Recent studies have shown significant influence of PBL parameterizations on moisture transport and ultimately, the diurnal cycle of precipitation, over the Andes-Amazon transition region (Hu et al., 2023; Huang et al., 2023; Martinez et al., 2022). Previous 3-month simulations showed that the Yonsei University (YSU, Hong et al., 2006) and the Asymmetric Convective Model v2 (ACM2, Pleim, 2007) schemes exhibited large differences in precipitation in regional climate simulations over the Andes-Amazon transition region (Hu et al., 2023; Huang et al., 2023). Such sensitivity is associated with differences in treatments of turbulence-cloud-precipitation processes in both the PBL and free troposphere within the YSU and ACM2 schemes. In addition, Martinez et al. (2022) showed that the YSU scheme simulates stronger low-level jets than the Mellor-Yamada-Nakanishi-Niino 2.5 scheme (MYNN, Nakanishi and Niino, 2009), although the results were centered over the equatorial and northern South America. Thus, we first study the sensitivity of the diurnal cycle of precipitation over the Quincemil hotspot under the YSU, ACM2 and MYNN PBL schemes, and we select the best scheme under which precipitation over the Quincemil hotspot is best resolved.

One of the main variables under analysis is the integrated water vapor transport (IVT) and its convergence. For the former, its formulation is represented in the following equation:

$$IVT = -\frac{1}{g}\int_{psfc}^{ptop}(uq + vq).dp \quad (1)$$

In Eq. (1), q is the specific humidity, u and v are the zonal (x) and meridional (y) components of the wind, respectively, p is the pressure level, psfc is the surface level, ptop is the top of the atmospheric layer (50 hPa), and g is the acceleration due to gravity. IVT is calculated by the summation of water vapor transport over the pressure levels using finite centered differences in the vertical dimension. Its units are in $kg{\cdot}m^{-1}{\cdot}s^{-1}$.

Similarly, IVT convergence is calculated as Eq. (2) by using finite centered differences on a lat/lon (x-y) grid. Its units are in $kg{\cdot}m^{-2}{\cdot}s^{-1}$

$$IVT\ convergence = -\frac{1}{g}\int_{psfc}^{ptop}\left(\frac{\partial uq}{\partial x} + \frac{\partial vq}{\partial y}\right).dp \quad (2)$$

Next, we perform topographic sensitivity experiments, which are listed in Table 3, and the correspondent model altitudes are illustrated in

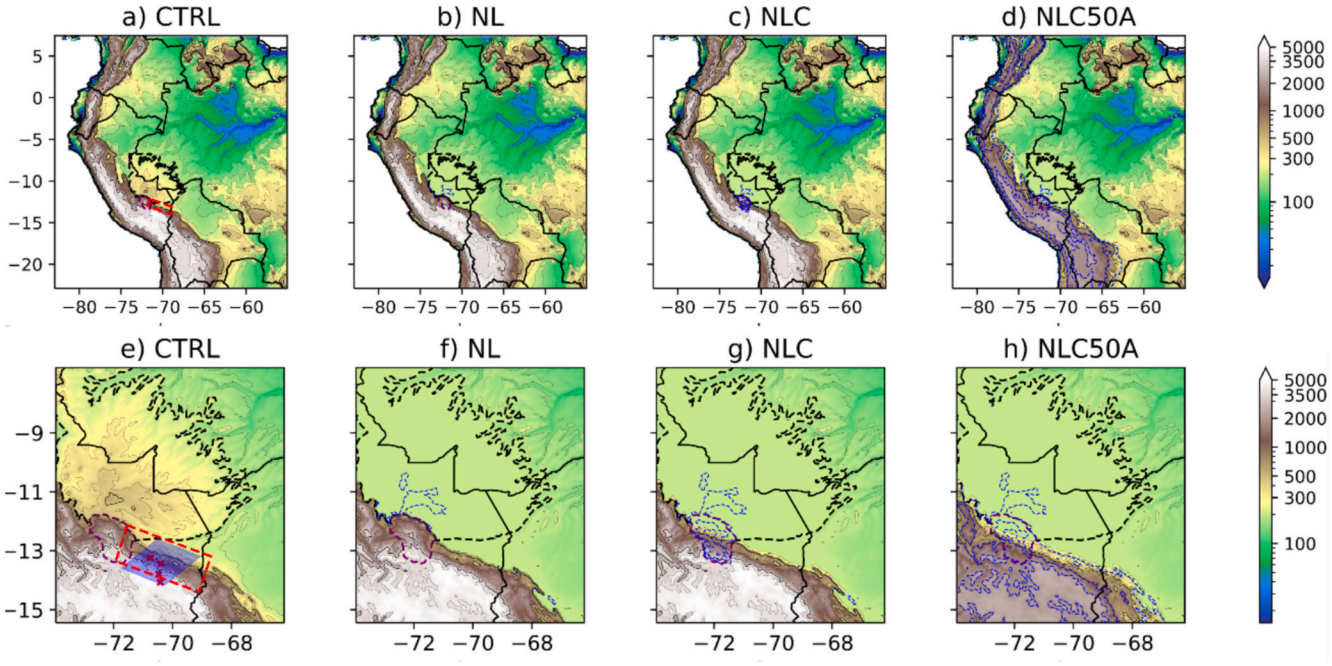

Fig. 2. First and second domain altitudes for each topographic sensitivity experiment. The black and purple dashed lines represent the Fitzcarrald arch and Camisea mountain, respectively, while the dashed red rectangles in both a) and e) represent an approximate location of the Quincemil hotspot. In 2e, blue oblique lines represent the transects followed across the Quincemil hotspot, and the red crosses represent the weather stations locations across them. Blue dashed lines represent differences of −250, −1000 and −2500 with respect to CTRL. (For interpretation of the references to color in this figure legend, the reader is referred to the web version of this article.)

Table 4
Model set-up and physical parameterization tests of the carried topographic sensitivity experiments (see corresponding altitudes in Fig. 2). The CTRL conditions were obtained after a sensitivity analysis of three PBL parameterizations (Table 3), where the best simulation of the diurnal cycle of precipitation over the Quincemil hotspot is chosen.

Topographic sensitivity experiment	Complete description
CTRL	Control
NL	No Lowlands
NLC	No Lowlands + No Camisea
NLC50A	No Lowlands + No Camisea + 50 % Andes

Fig. 2. The control simulation ("CTRL") is constituted by the best of the three PBL sensitivity experiments. The sensitivity experiments were conducted by changing different topographic structures, and comparing them to CTRL. In the "No Lowlands" experiment (hereafter called NL), we remove the lower part of the Fitzcarrald arch, being flattened to an altitude of 200 m.a.s.l., to isolate its effect (Fig. 2b, f). 200 m.a.s.l. is chosen as an approximate height of the adjacent Amazonian regions to the Fitzcarrald arch. In the "No Lowlands + No Camisea" experiment (hereafter called NLC; Fig. 2c, g), in addition to the removal of the arch, we removed the Camisea mountains, which are associated with the formation of the Fitzcarrald arch (Espurt et al., 2007). The NLC50A experiment is like the NLC experiment but, in addition, the Andes is reduced to 50 % of its altitude (Fig. 2d, h). This fraction is selected as inspired by paleo-altitudes of the Andean range of 5–10 million years ago (Garzione et al., 2017), at the beginning of the formation of the Fitzcarrald Arch (Table 4).

It is worth mentioning that the scope of the topographic sensitivity experiments is primarily on the response of atmospheric mechanisms and rainfall around the Quincemil hotspot. Regional changes are also appraised in the NLC50A experiment. However, this investigation does not aim to explore changes in global atmospheric mechanisms as a consequence of reducing the Andes in half (NLC50A).

3. Model validation

In this section, we validate the simulated diurnal cycle of precipitation over the Quincemil hotspot region using three satellite products and rain-gauge measurements. We focus on the region around the Quincemil hotspot, and we use the WRF model output from the second domain. From the satellite estimations, important differences are noticeable

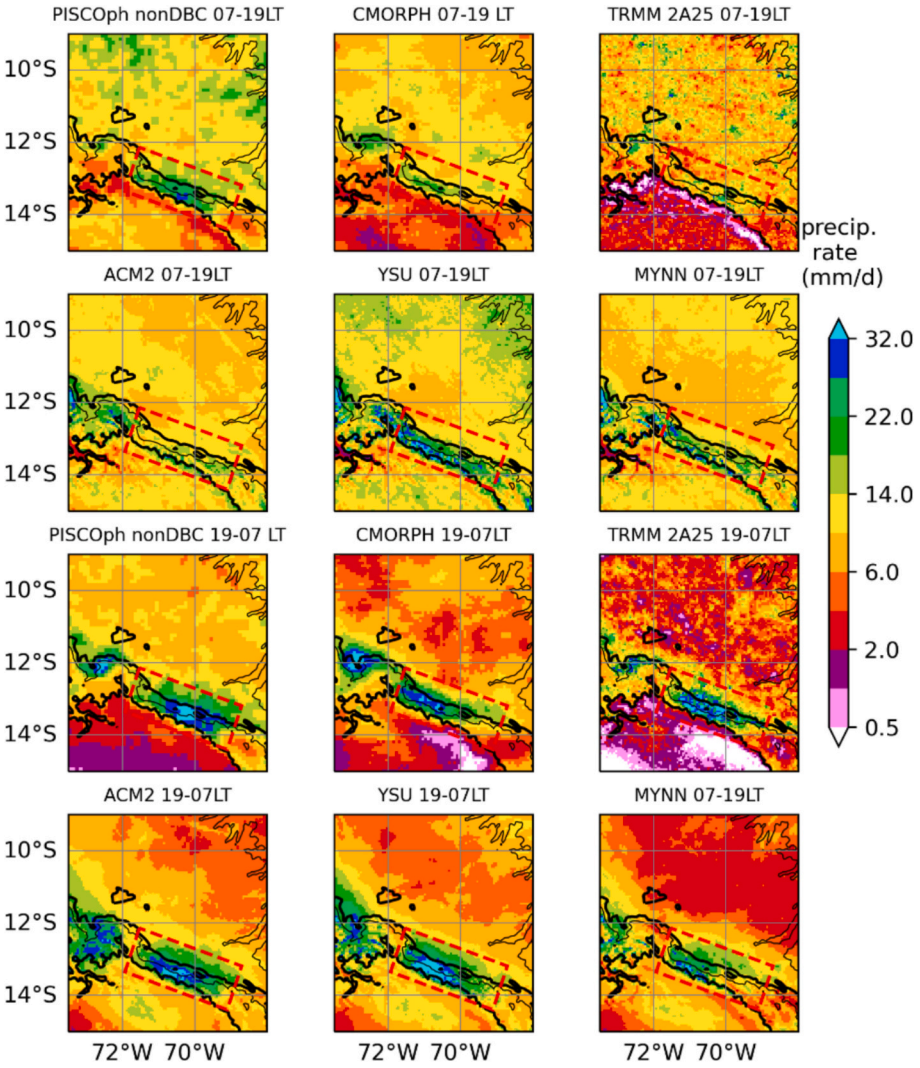

Fig. 3. Precipitation rates (mm/d) derived from observational gridded datasets (first and third rows) and simulated by parameterization tests (second and four rows) during daytime (07-19LT, first two rows) and nighttime (19-07LT, third and fourth row). Note that the DJF 2015–20 and DJF 2000–14 averages are shown for PISCOph and TRMM 2A25 products, while DJF 2012–13 is shown for CMORPH. Black lines represent the altitudes of 200, 500, 1000 and 3000 m.a.s.l. The dashed red rectangles represent an approximate location of the Quincemil hotspot. (For interpretation of the references to color in this figure legend, the reader is referred to the web version of this article.)

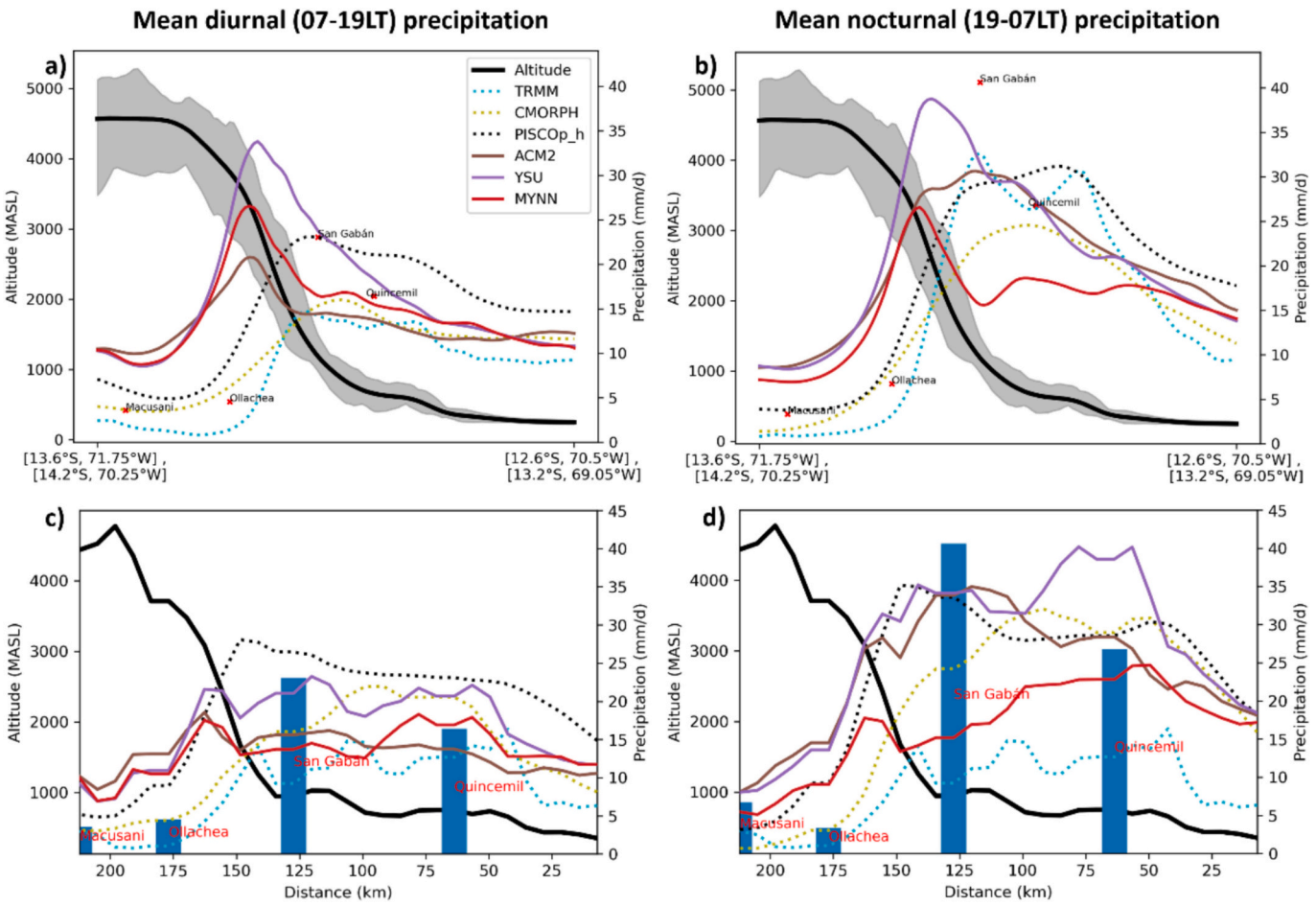

Fig. 4. Mean precipitation-elevation cross sections across the transects over the Quincemil hotspot delineated in Fig. 2e (a, b) and across the transects delineated in Fig. 1b (c, d) Diurnal precipitation averages (07-19LT) are shown in a, c, while nocturnal precipitation means (19-07LT) are shown in b, d. Observational gridded datasets are delineated by dotted lines, and parameterization tests by solid lines. Mean altitude (WRF) across the transects are illustrated by thick black lines. In a, b, the altitude spread (minimum/maximum) across each transect point is shown as a gray envelope and red crosses represent the altitude, location and daily precipitation average for the stations located across the transects (see Fig. 2e). In c, d, blue bars represent the altitude, location and diurnal/nocturnal precipitation averages for the stations located across the transects (see Fig. 1b). Note that the DJF 2015–20 and DJF 2000–14 averages are shown for PISCOph and TRMM 2A25 products, while DJF 2012–13 is shown for CMORPH. (For interpretation of the references to color in this figure legend, the reader is referred to the web version of this article.)

between daytime and nighttime conditions (first and three rows of Fig. 3). In the eastern slope of the Andes between 3000 and 500 m.a.s.l. (including the Quincemil hotspot), summertime rainfall tends to occur during all day, but with a stronger maximum during the night. However, in the Andean highlands above 3000 m.a.s.l., and the Amazonian plains, the precipitation maxima occurs during the day (Chavez and Takahashi, 2017; Junquas et al., 2018). While there are significant quantitative differences between satellite estimations, they all agree with this spatial pattern.

Regarding the model, the three performed PBL sensitivity experiments were able to broadly reproduce this pattern (second and fourth row of Fig. 3). However, some quantitative biases over the Quincemil hotspot arise in these simulations. First, a significant daytime overestimation of 300 % and 450 % of rainfall rates observed by PISCOp_h in altitudes between 3000 and 4000 m.a.s.l. occurs in the MYNN and YSU simulations, respectively. This bias is partially mitigated under the ACM2 simulation, which is also evident in the spatially averaged cross sections in Fig. 4a. Second, the intensity and spatial extension of the nocturnal Quincemil hotspot differs significantly between the PBL sensitivity simulations. Although there are also important differences between satellite products, nighttime rainfall over the Quincemil hotspot is underestimated by the MYNN simulation (~15 mm/d with respect to PISCOp_h). In addition, YSU simulates a very strong nocturnal hotspot, where grids with >32 mm/d are present in altitudes above 3000 m.a.s.l, while at this altitude all products show values less than 20 mm/d (Fig. 4b). The ACM2 simulation, on the other hand, is contained within the variability of the satellite products for both day and night below 3000 m, which can also be seen in the spatially averaged cross sections over Quincemil in Fig. 4, and it is the simulation with less daily over-estimation above 3000 m (Fig. 4a–b). When model biases are quantified against CMORPH for DJF 2012–13 (the only product with a common time period with simulations), the validation metrics yield inconclusive results. While the ACM2 simulation appears to exhibit lower biases during daytime, none is markedly better at nighttime (Fig. S1 and Tables S1–S2).

When taking into account a fixed route following the rain-gauges locations instead (Fig. 4c–d), we find similar biases in the PBL sensitivity experiments. Interestingly, the YSU and ACM2 experiments are able to capture the nocturnal rainfall maximum around the location of the San Gabán station better than the satellite estimations (Fig. 4d). Nonetheless, a denser rain gauge network would be required to validate such rainfall gradients.

It should be noted that we do not explore how regional and mesoscale processes change due to the PBL scheme choice near Quincemil, and how these differences interact with the removal of topography in the following sensitivity experiments. Nevertheless, the sensitivity of these

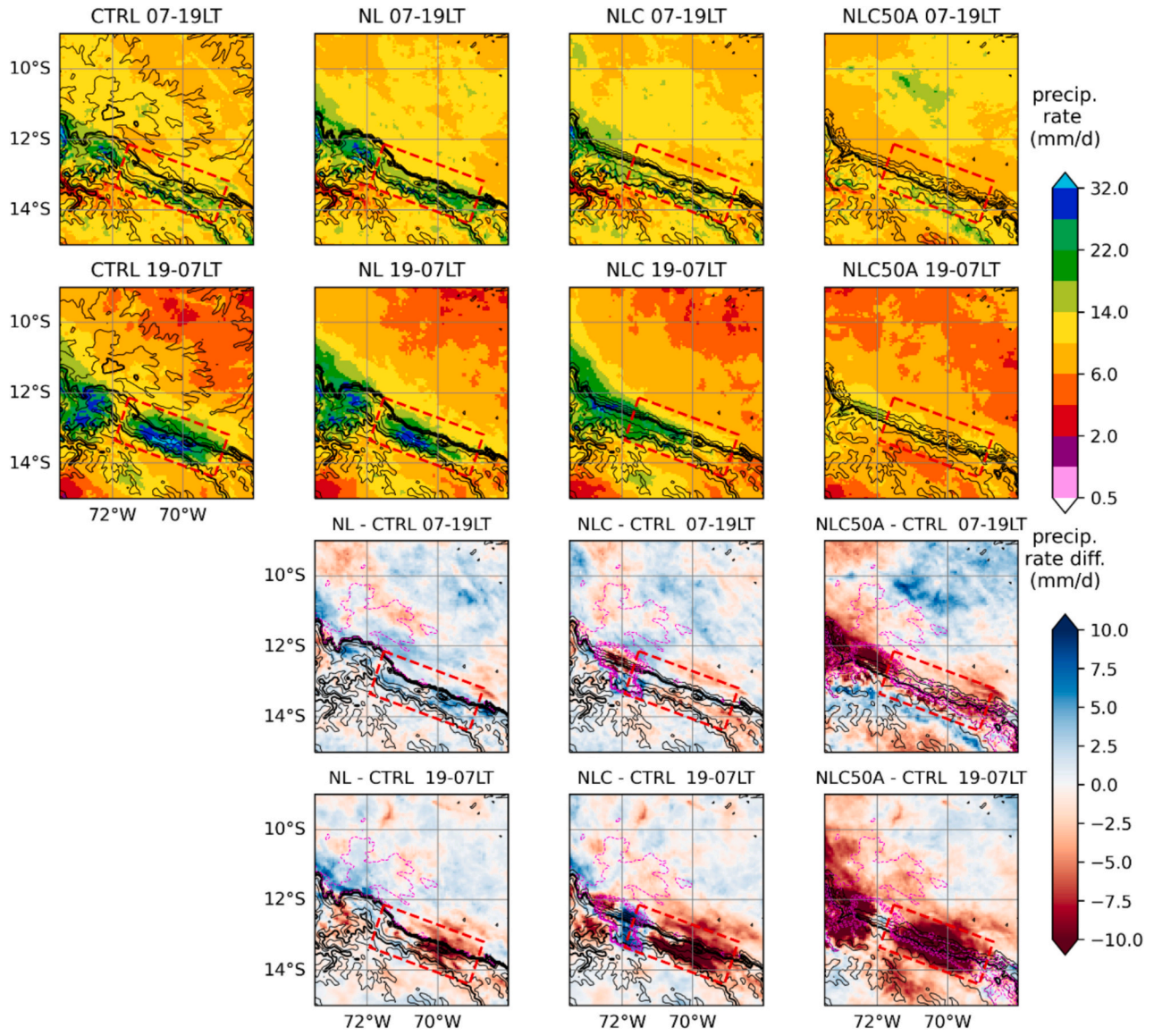

Fig. 5. Diurnal and nocturnal precipitation rates simulated by topographic sensitivity experiments (first and second row, respectively). Differences with respect to CTRL are shown in the third and fourth row. Black lines represent the altitudes of 50, 100, 150, 200, 300, 400, 500, 600, 1000, 2000, 3000 and 4000 m.a.s.l., with 500 and 3000 m.a.s.l. as thick black lines. Magenta lines show altitude differences with respect to CTRL of −200, −400, −600, −800 and −1000 m.a.s.l. The dashed red rectangles represent an approximate location of the Quincemil hotspot. (For interpretation of the references to color in this figure legend, the reader is referred to the web version of this article.)

mechanisms to PBL parameterizations over the western Amazon have been investigated before (e.g., Hu et al., 2023; Huang et al., 2023; Martinez et al., 2022). Here, we prioritize the preservation of the spatial coherence of the diurnal cycle of rainfall over the Quincemil hotspot, thus choosing the ACM2 simulation as our CTRL simulation for the remainder of this study, using the ACM2 scheme as the selected PBL parameterization.

4. Influence of topographic features

4.1. Diurnal cycle of precipitation

In this section, we start analyzing the topographic sensitivity experiments in terms of the diurnal cycle of precipitation in the d02 domain (spatial resolution of 5 km). The removal of the Fitzcarrald arch in NL is associated with a slight increment on diurnal rainfall around the Quincemil hotspot (~3 mm/d), but stronger diminutions on nocturnal rainfall at the core of the Quincemil hotspot (around 8 mm/d, second column in Fig. 5). When also removing the Camisea mountains in the NLC experiment, such nocturnal diminutions are even stronger, with values approximately 15 mm/d lower than in CTRL.

Additionally, at the west of the original Quincemil hotspot location, where the Camisea mountains were located, precipitation increases to values above 18 mm/d, due to a westward shift of the hotspot. This constitutes a reduction of about 40 % of precipitation over the Quincemil hotspot. When reducing the altitudes of the Andes by 50 % in NLC50A, the strongest diminutions are found, virtually removing the Quincemil hotspot from the simulation by reducing about 60 % of precipitation. The spatially averaged cross-section over Quincemil corroborates such results (Fig. 6). The cross-section derived from NLC exhibits a double-peaked precipitation profile. The lower altitude maximum might appear as the extension of a western-migrated rainfall hotspot, which now is located closer to the removed Camisea mountains. It is worth noting that the only experiment that exhibits significant changes in daytime precipitation over the Quincemil hotspot is NLC50A (Fig. 6a), while important reductions in nocturnal precipitation arise in

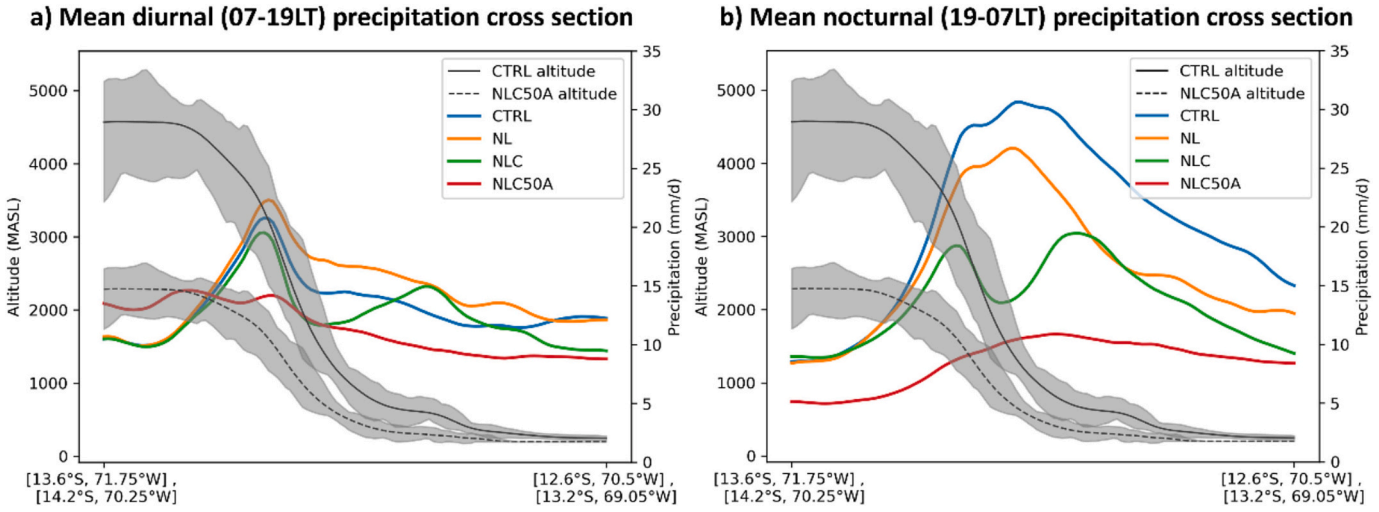

Fig. 6. Mean precipitation-elevation cross sections for four topographic sensitivity experiments across the transects over the Quincemil hotspot delineated in Fig. 2e. Diurnal precipitation means (07-19LT) are shown in a), while nocturnal precipitation means (19-07LT) are shown in b). Mean CTRL (NLC50A) altitude across the transect is illustrated by solid (dashed) black lines, and their spreads (minimum/maximum) across each transect point are shown as gray envelopes. Note that NL and NLC profiles are not shown as the constructed transects do not pass through modified terrain (Fig. 2) and they would be very similar to CTRL.

all of the experiments (Fig. 6b).

4.2. Local changes in moisture transport, relative vorticity and mountain circulations

Given that the most significant changes in precipitation occur during nighttime, we focus on the atmospheric physical mechanisms occurring during the night. The nighttime integrated water vapor transport (IVT) and its convergence are shown in Fig. 7. The IVT convergence in CTRL (Fig. 7a) is consistent with nighttime precipitation regions in Fig. 5, located on the eastern Andean slopes between 500 and 3500 m.a.s.l. The averaged SALLJ structure is also evident from the strong northwesterly moisture transport. In addition, the direction of IVT relative to the axis of the Andean cordillera was previously proposed as a hotspot-related process associated with the spatial maximum of precipitation and increased convergence in the eastern Andean slopes (Espinoza et al., 2015; Junquas et al., 2018).

With the removal of the Fitzcarrald arch in the NL experiment (Fig. 7b, f), the IVT convergence around the Quincemil hotspot is reduced, consistent with nocturnal rainfall diminution seen in Fig. 5. Under the NLC experiment (Fig. 7c, g), IVT convergence around the Quincemil hotspot experiences stronger reductions than under NL, and it is associated with an anticyclonic-like IVT anomaly around the concavity of the removed Camisea mountain. The direction of the SALLJ-associated IVT relative to the axis of the Andean cordillera is more parallel around Quincemil due to such IVT anomalies which, combined with the reduced convergence, considerably reduces nocturnal rainfall around Quincemil (Fig. 5).

Finally, under the NLC50A experiment, SALLJ-associated IVT over the entire domain is greatly diminished, and the reductions on IVT convergence yield very strong reductions of precipitation over the Quincemil hotspot (Fig. 5). Such results are consistent with Insel et al. (2010), who performed regional climate simulations with reduced values of modern Andean heights. In addition, the removal of the Camisea mountains in this experiment might also provide another source of diminution of IVT and its convergence, although regional scale anomalies appear to be dominant.

We now explore changes in 850 hPa winds and relative vorticity (Fig. 8). This pressure level is commonly analyzed as it is representative of large-scale moisture transport towards the rainfall hotspots (e.g., Chavez and Takahashi, 2017; Espinoza et al., 2015). The characteristics of the average nocturnal 850 hPa in CTRL and their differences in the experiments are similar to those from IVT in Fig. 7. In CTRL, the negative relative vorticity values downstream the Camisea mountains towards the Quincemil hotspot further illustrate the possible role of local topography in providing a local atmospheric dynamic trigger to convection around the Quincemil hotspot. Under the NL experiment, there is a very slight reduction in relative vorticity associated with the removal of the Fitzcarrald arch. However, significantly greater diminutions in this variable occur with the removal of the Camisea mountains under NLC and NLC50A. Since the maximum altitude of the Camisea mountain is around 700 hPa (~3000 m a.s.l.), it could be expected that the greatest diminutions are found in low pressure levels. This diminution is consistent with the reductions of IVT convergence in Fig. 7, leading to significant reductions in nocturnal rainfall under such experiments (Fig. 5).

We also considered changes in the vertical structure of wind speed over Cobija, a Bolivian city located at the Amazon lowlands along the SALLJ stream (Marengo et al., 2004). Wind speeds in the lower and mid troposphere are the most sensitive in the performed experiments, where a maximum of ~7.2 m/s is found around 750–800 hPa in CTRL (Fig. 7e). Slight decreases are found in NL, while stronger reductions in wind speed are found in NLC. However, the most profound reductions in wind speed occur under NLC50A between 500 and 900 hPa. The strongest wind shear changes can also be found under this experiment, where the maximum is now located at 925 hPa. This is coherent with the weakening of lower-to-middle tropospheric meridional winds found in similar experiments by Insel et al. (2010) and Saurral et al. (2015). Wind speeds quickly decrease with altitude, showing a maximum reduction of ~40 % in 750 hPa. This is consistent with the strong IVT reductions found in NLC50A (Fig. 7h). The 500–900 hPa layer corresponds to the presence of a SALLJ-like structure in the simulations, and the maximum reduction in 750–800 hPa also corresponds to the maximum of the SALLJ-like wind speed observed during the SALLJEX experimental campaign (Vera et al., 2006b; Yabra et al., 2022). Such reductions could be caused by the reduced capability of the Andes to block the synoptic flow in the NLC50A experiment.

When further analyzing changes in a longitudinal vertical cross section around the Quincemil hotspot, we find reductions in specific humidity of around 0.2 g/kg below 750 hPa in NL and below 0.4 g/kg below 700 hPa in NLC (Fig. 9). Such changes are associated with reductions in vertical velocity across the vertical profiles around Quincemil, especially in NLC (Fig. 9f). Furthermore, stronger diminutions in specific humidity (~1 g/kg) are found in NLC50A between the 400 and

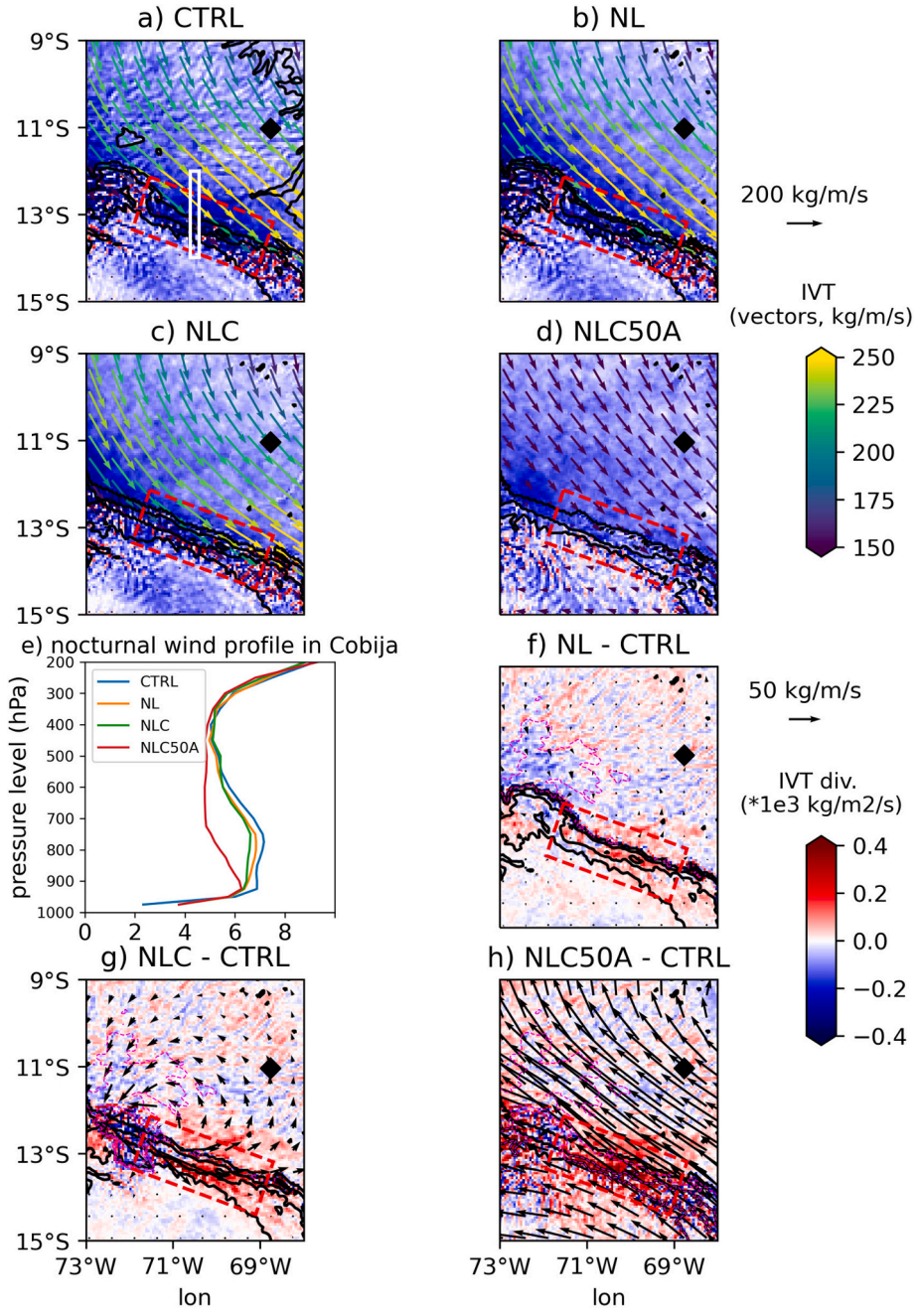

Fig. 7. Nocturnal moisture transport over the Quincemil hotspot in topographic sensitivity experiments. Mean fields of nocturnal IVT and its divergence (a–d), and differences with respect to CTRL (f–h). The black diamonds in 68.77°W and 11.03°S in a–d and f–h represent the location of Cobija. e) Average vertical profiles of nocturnal wind speed in Cobija. The reference vector for each row is the one at its rightmost side. Black and thin lines in f–h delineate the altitudes of 200, 500, 1000 and 3000 m.a.s.l. The white path in a) shows the region where the cross sections shown in Fig. 9 are constructed.

850 hPa layer, in association with stronger decreases in vertical velocity around Quincemil (Fig. 9g). In addition, strong southerly anomalies in meridional winds, of up to 3 m/s, are found at 700 hPa.

Thus far, only the nocturnal atmospheric mechanisms have been discussed, as the most significant changes in precipitation occurring during the night (see Section 4.1). Changes in daytime atmospheric mechanisms are similar of those during the night, especially those regarding regional scale moisture changes, which are more noticeable in NLC50A (Figs. S4–S6). However, some important differences arise when analyzing the cross section constructed in Fig. 9 (Fig. S8). During the day, reductions in moisture content and vertical velocity are more confined to the mountain surface compared to nighttime conditions, resembling anabatic winds; whereas at night it becomes stronger and extends over a broader atmospheric layer (Fig. 9). This suggests that the modification of the terrain in our experiments might produce important changes in the thermal forcing that originates local scale mountain circulations, which manifests in diurnal differences in mentioned motions. However, previous studies suggest that both thermal-induced circulations and SALLJ-associated moisture transport during the night contribute to approximately 70 % of total precipitation around the Quincemil hotspot (Chavez and Takahashi, 2017; Espinoza et al., 2015; Junquas et al., 2018). Both processes might have been weakened in our simulations, which helps to explain the greater reductions in nocturnal rainfall over the Quincemil hotspot. Nevertheless, the interaction of changes induced by the Andean terrain modification in the thermal forcing and in the regional scale atmospheric circulation remain to be

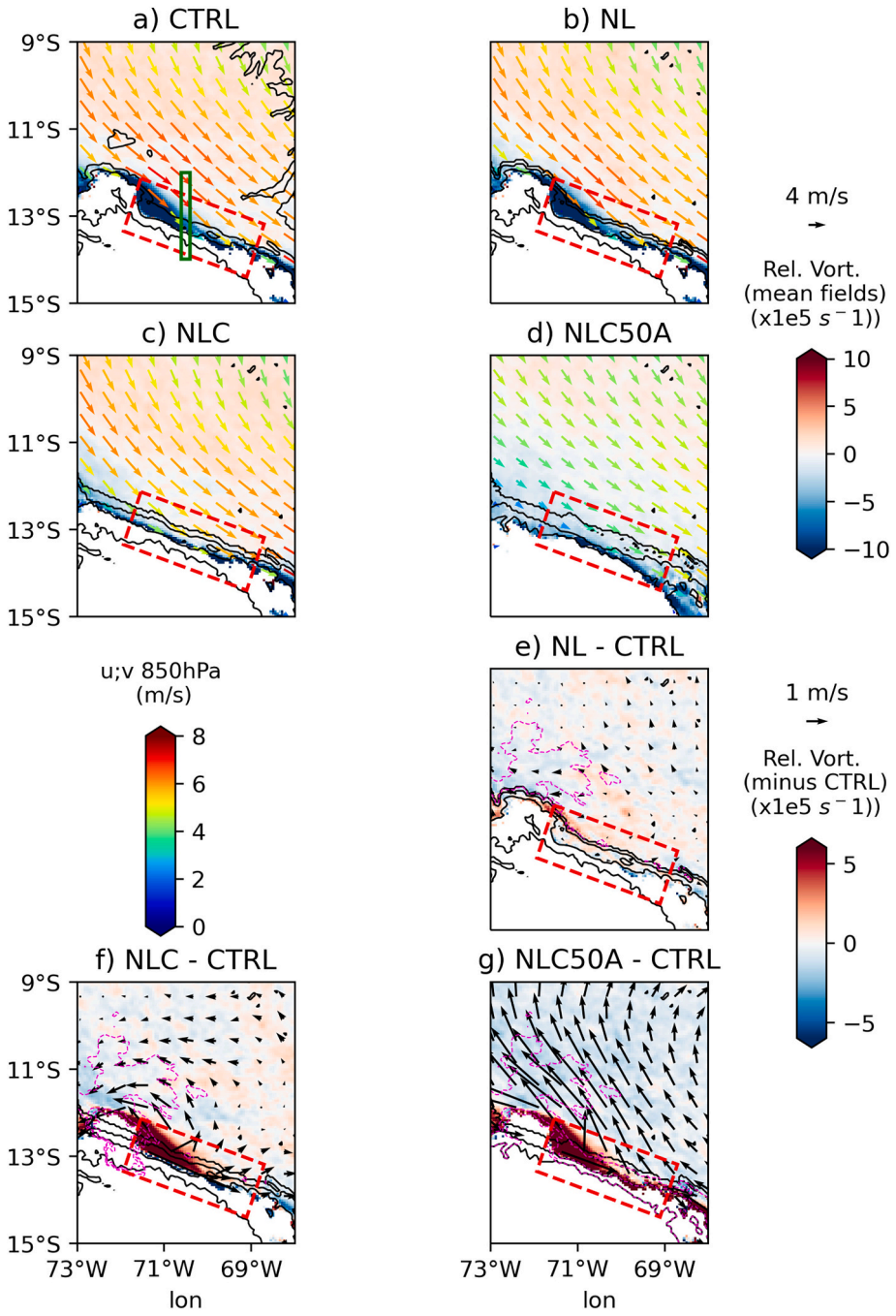

Fig. 8. 850 hPa winds and its rotational component over the Quincemil hotspot in topographic sensitivity experiments. Mean fields of nocturnal 850 hPa winds and their relative vorticity (first and second rows), and differences with respect to CTRL (third and fourth rows). The reference vector for each row is the one at its rightmost side. Black and thin lines in the second row delineate the altitudes of 200, 500, 1000 and 3000 m.a.s.l. Magenta lines show altitude differences with respect to CTRL of −200, −500 and −1000 m.a.s.l. The white path in a) shows the region where the cross sections shown in Fig. 9 are constructed. (For interpretation of the references to color in this figure legend, the reader is referred to the web version of this article.)

disentangled.

4.3. Regional scale changes in moisture transport

In this section, we discuss the climate impacts of changing the Fitzcarrald arch, Camisea mountain and the overall Andes altitudes upon the regional-scale climate (near and beyond the vicinity of the topographic modifications). We focus on the regional scale changes induced by the topographic sensitivity experiments in both precipitation and moisture transport by analyzing the d01 domain (spatial resolution of 15 km). The removal of the Fitzcarrald arch in both NL and NLC experiments seems to have an impact in regional climate by producing an increase in rainfall centered at around 12°S 63°W, to the east of a modern wetland known as Llanos de Moxos (Fig. 10 and Fig. 1a). In addition, with the removal of the Fitzcarrald arch, the Camisea mountains, and the overall reduction of the Andes by 50 % in NLC50A, significant reductions in rainfall are also evident in the regional scale across the eastern Andean slopes between 7°S and 18°S. These are the locations of other precipitation hotspots identified in previous studies (e.g., Espinoza et al., 2015) and reproduced by the model in CTRL.

Because the most significant changes in precipitation occur during nighttime, we further analyze changes in nocturnal IVT and its

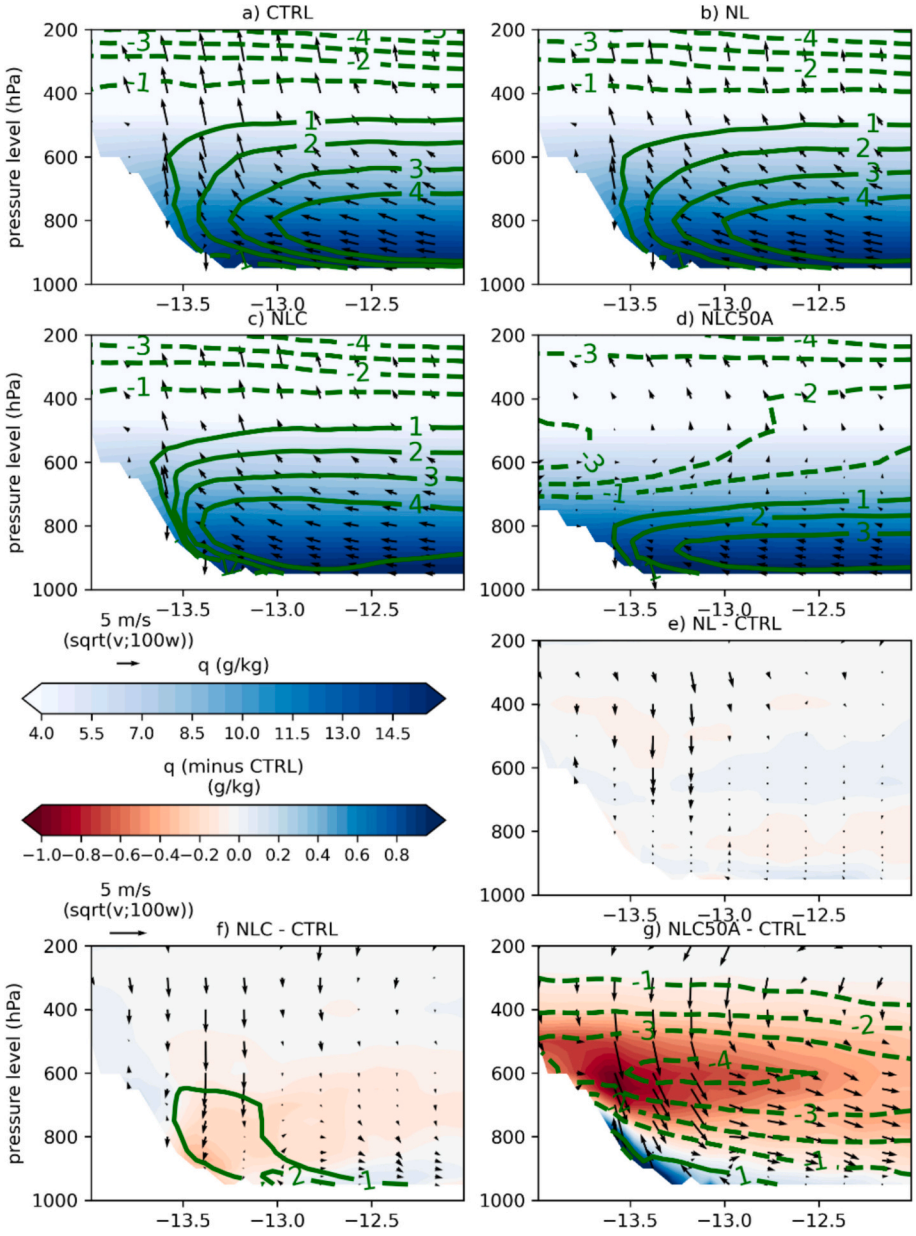

Fig. 9. Nighttime-averaged (19-07LT) vertical cross sections between 70.4°S–70.6°S and 12°S–14°S (white box in Figs. 7–8) of meridional-vertical winds (vectors), specific humidity (colorbars) and zonal winds (contours). These vectors/magnitudes are shown in terms of averages for each topographic sensitivity experiment (a–d) and in terms of differences with respect to CTRL (e–g) (For interpretation of the references to color in this figure legend, the reader is referred to the web version of this article.).

convergence in the d01 domain (Fig. 11). Local topographic changes in both NL and NLC induce a wave-like response in IVT in the western-southern Amazon, and a cyclonic anomaly (Fig. 11f, g) around 15°S–63°W explains the positive rainfall anomalies simulated around eastern Llanos de Moxos seen in Fig. 10. For NLC, the local anticyclonic-like anomaly around Quincemil seen in Fig. 7 for the d02 domain can be found, and it is associated with a cyclonic-like anomaly centered at 15°S–61°W.

Regional-scale effects dominate in the first domain of NLC50A when compared to CTRL, as seen in the southerly IVT anomalies across the eastern flank of the Andes and associated IVT convergence reduction in that region (Fig. 11d, h). At the western Amazon, IVT is reduced by 20–60 %, with higher reductions closer to the Andes-Amazon transition region. Such results are consistent with Insel et al. (2010) and Junquas et al. (2016), who completely removed the Andes in a two-way nested general circulation model. Our results might be associated with the weakening of the mechanical forcing of the intensity of the SALLJ by the Andes. The weakening of the SALLJ in NLC50A might explain why the Quincemil hotspot practically disappears from the simulation, whereas in NLC there is still a weakened hotspot. This suggests that the height of the Andean cordillera is a factor that influences the intensity of not only the Quincemil rainfall hotspot, but all the rainfall hotspots in the eastern flank of the Andes, via its regional impact on the moisture transport.

When analyzing the vertical structure of wind speeds over Santa Cruz de la Sierra, one of the main locations used to study SALLJ form and variability (Marengo et al., 2004; Montini et al., 2019), a vertical maximum of 12 m/s appears around 800–850 hPa in CTRL (Fig. 11e). While mild increases in wind speed appear in NL and NLC, the strongest changes occur in NLC50A, as found in Fig. 7 for the d02 domain. While in NLC50A the vertical structure is somewhat similar to CTRL, reductions of up to 45 % are simulated between 600 and 900 hPa. This is consistent with the significant reductions found in NLC50A with respect

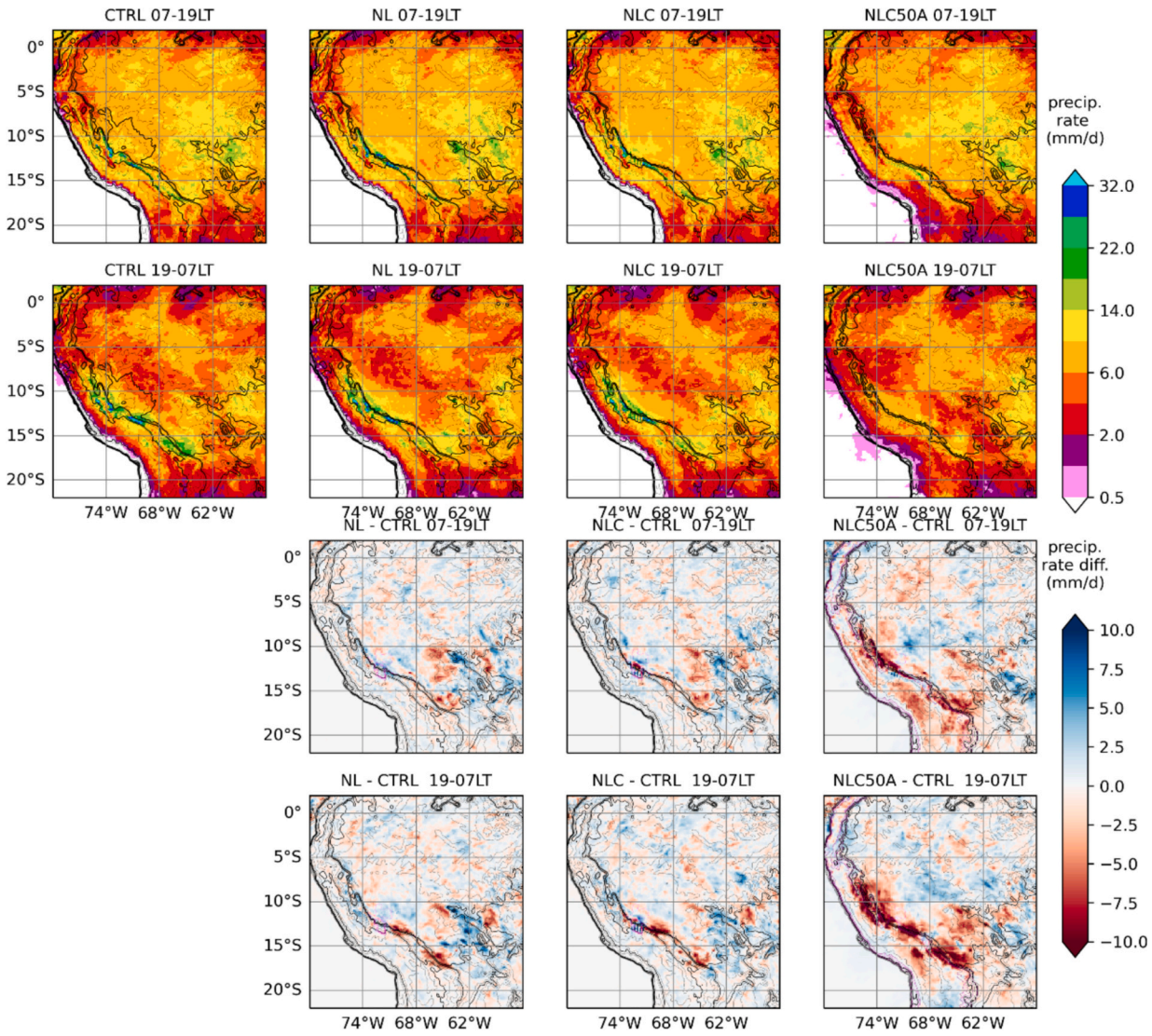

Fig. 10. As Fig. 5, but considering the output from the d01 domain.

to CTRL in Fig. 11h.

5. Discussion and conclusions

In this study, we assess the role of local topographic features in the rainiest region of the Andes-Amazon transition zone on the summertime atmospheric mechanisms associated with the Quincemil precipitation hotspot in topographic sensitivity experiments using the WRF model. We schematized the main findings of this paper in Fig. 12. Our results indicate that such features, namely, the Fitzcarrald Arch and the Camisea mountains, both related to the Nazca Ridge subduction (Espurt et al., 2007, 2009), play an important role in the modulation of the location and intensity of the Quincemil hotspot. The associated atmospheric mechanisms are linked to modulations in the moisture flux and its convergence towards the eastern Andean slopes between 500 and 3500 m.a.s.l., where the Quincemil hotspot is located. These mechanisms are local scale-induced, where the Fitzcarrald Arch (NL) and both the Fitzcarrald Arch and the Camisea mountain (NLC) account for about 16 % and 40 % of rainfall amount over the Quincemil hotspot, respectively. These factors not only affect the intensity of the Quincemil hotspot, but also its location. This especially happens for the Camisea mountain, as the vortical-induced circulations due to its concavity can also channelize the moisture flux towards the Quincemil hotspot and serve as a trigger to convective processes over this region (thin blue arrows in Fig. 12a–b). When including a reduction in 50 % of the modern Andean heights on top of the removal of mentioned features, we find a significant role of the Andes in modulating moisture fluxes over the Andes at the regional scale (dashed red arrows in Fig. 12d). This factor controls as much as 60 % of total rainfall in the eastern flank of the Andes, and is decisive in the simulation of rainfall hotspots at the Andes-Amazon transition region. Such modulation is consistent with previous topographic sensitivity experiments, where it was found that the Andes serves as a mechanical forcing to SALLJ-associated moisture flux (Insel et al., 2010; Junquas et al., 2016; Saurral et al., 2015).

In this paper, we have used simulations at a spatial resolution of 5 km with parameterized convection. Recent developments in regional climate modeling have made use of convection-permitting simulations, where kilometer-scale simulations (finer than 5 km) allow for a more explicit representation of convective processes by deactivating convective parameterization (e.g., Dominguez et al., 2023; Junquas et al., 2022). In principle, it could be useful to alleviate problems of coarser climate models with parameterized convection due to the greater detail in the representation of surface heterogeneity (Kendon et al., 2021), Nevertheless, these benefits might not be obvious over the tropical Andes.

Junquas et al. (2022) conducted one-year numerical experiments at

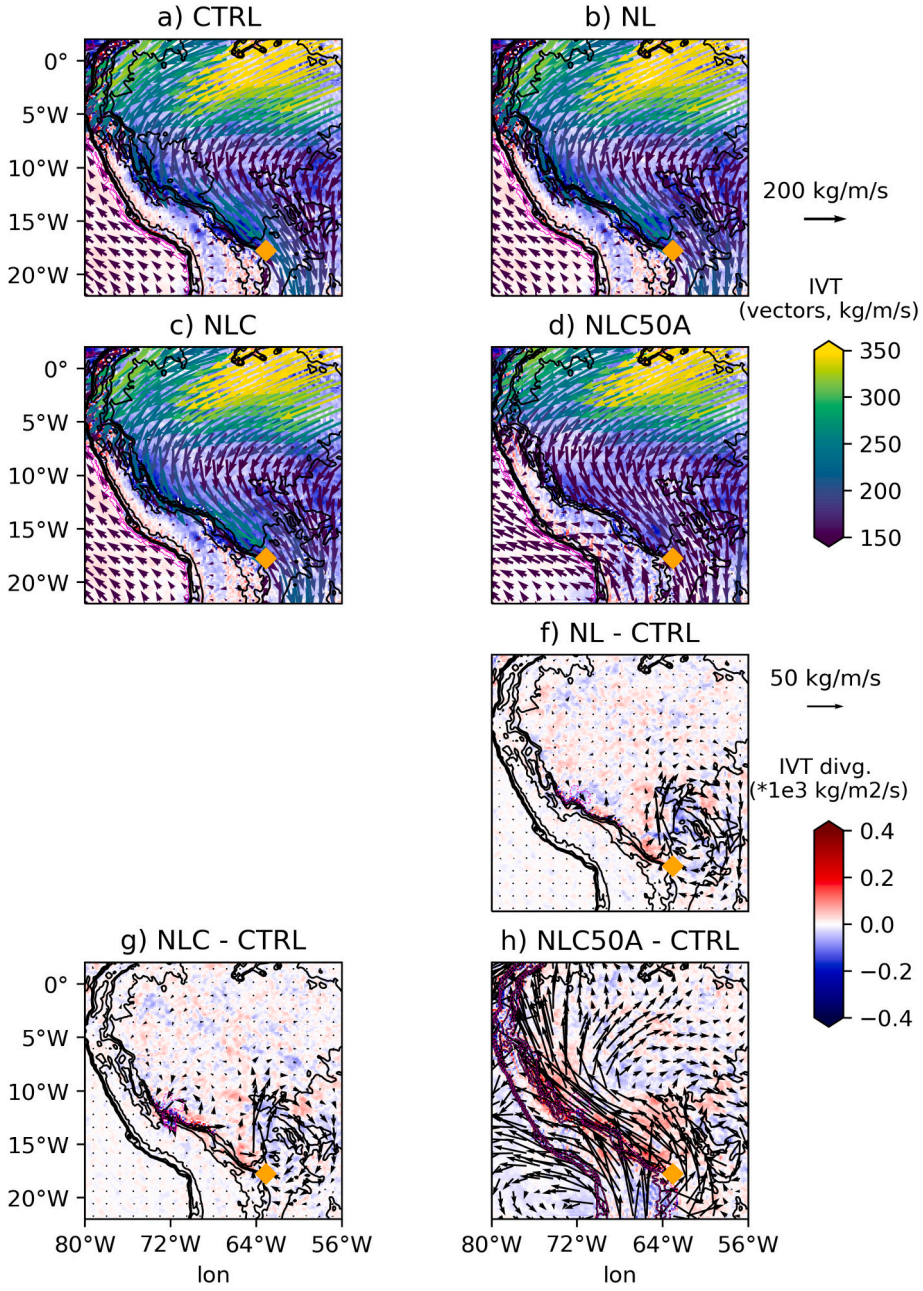

Fig. 11. As Fig. 7, but considering the output from the d01 domain. Orange diamonds represent the location of Santa Cruz de la Sierra (17.78°S, 63.08°W), where vertical profiles of nocturnal wind speed are constructed in e). Note that the x axis is scaled differently between Figs. 10e and 7f.

$\Delta x = 1$ km in the equatorial Andes and found that cumulus schemes still need to be activated at this resolution to properly capture the diurnal cycle of precipitation and its processes in the area. This suggests that certain convective and turbulent-scale processes over a tropical, topographically-complex region are still not fully represented within this framework at 1 km grid spacing, falling into the convective "gray zone". Further investigation is needed to assess the benefits or limitations of convection-permitting modeling over other tropical Andes locations, such as the Quincemil hotspot region, which can use a finer spatial resolution than the one used in this study.

We found significant impacts on vertical motions across the vicinity of the Quincemil hotspot in the topographic sensitivity experiments (especially in NLC50A), with noticeable differences between daytime and nighttime processes (Fig. 9 and Fig. S8). While during the day significant reductions in vertical velocity were found closer to the surface (in resemblance of anabatic winds), during the night they were stronger and covered a deeper atmospheric layer. We do not address thermally-driven processes in our experiments, but the sensible heat fluxes are proven to determine the precipitation distribution over the eastern flank of the Andes in sensitivity experiments (Junquas et al., 2018). In addition, topographic changes in the experiments could alter sun heating exposure and slope angles and distances, potentially introducing another local source of uncertainty in the simulation of anabatic and, especially, katabatic winds (Trachte et al., 2009).

The choice of the designed topographies for the sensitivity studies was based on previous studies on the origin and tectonic uplift evolution of the Fitzcarrald Arch, starting around 5–10 million years ago (Espurt et al., 2007, 2009), when the central Andean heights were at half of its modern values (Garzione et al., 2017). However, our experiments are not designed to be simulations of past timescales. Other evolving tectonic and climatic factors have certainly influenced the regional climate, including the continental drift of South America, changes in large-scale

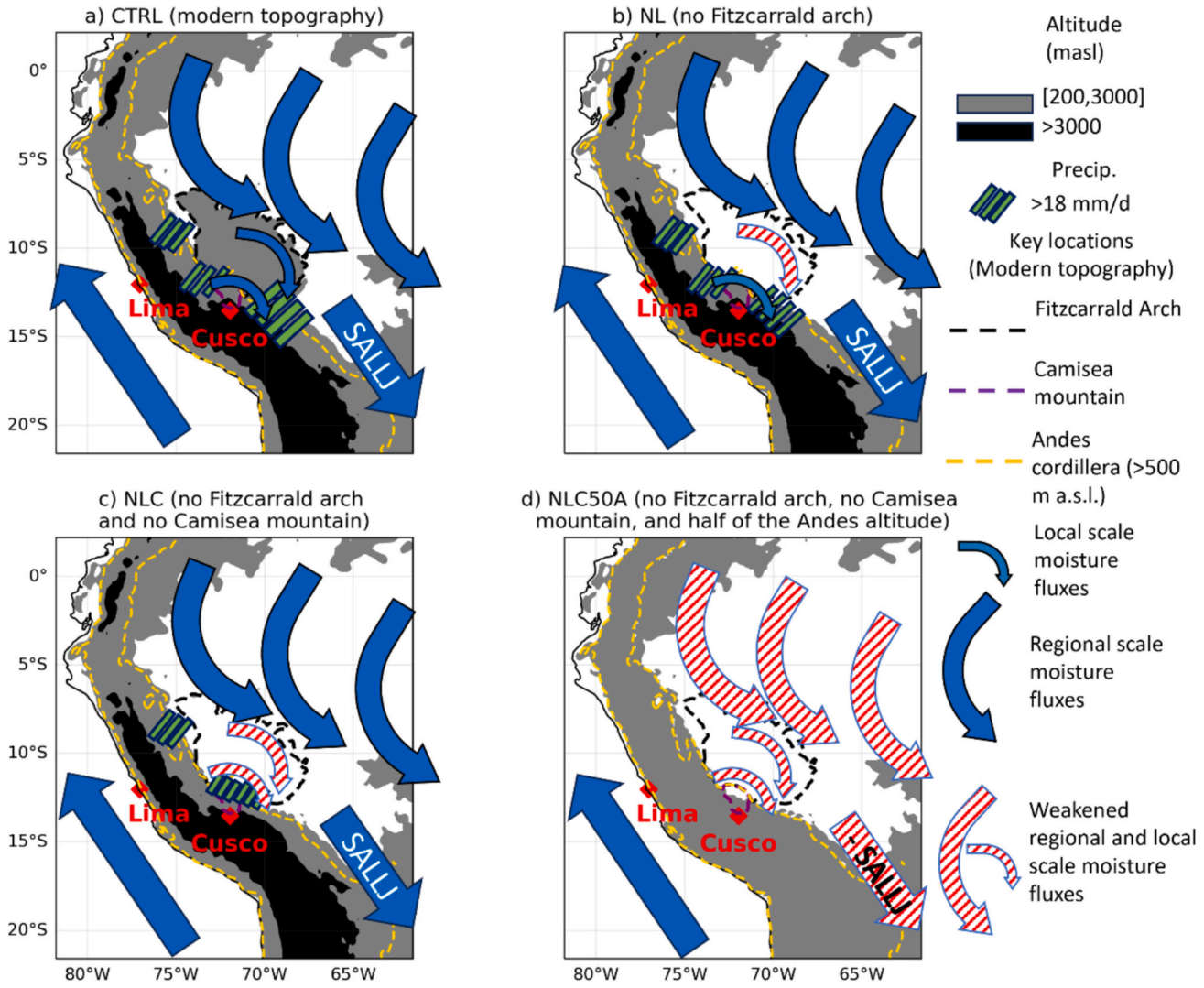

Fig. 12. A conceptual model regarding the role of local and regional scale topography on local and regional atmospheric circulation, and precipitation hotspots (precipitation rates >18 mm/d represented by green bars) during summer. Regions between 200 and 3000 m a.s.l. are bounded by a gray surface, while regions above 3000 m a.s.l. are depicted by a black surface. Regional and local scale moisture fluxes are shown as thick and thin arrows, respectively, in CTRL and in the topographic sensitivity experiments (b–d) if "unchanged" w.r.t. CTRL. Weakened moisture scale fluxes are shown as red dashed arrows. Key geographical locations under modern topography such as the Fitzcarrald Arch, the Camisea mountain and the Andes cordillera (altitudes higher than 500 m a.s.l.) are bounded by black, purple and gold dashed lines, respectively. The locations of key contemporaneous cities, Lima and Cusco, are depicted by red diamonds. (For interpretation of the references to color in this figure legend, the reader is referred to the web version of this article.)

oceanic circulation and sea surface temperatures, changes in atmospheric chemical composition, and changes in land surface characteristics. In addition to the removal of the Fitzcarrald arch and the Camisea mountain in NLC50A, we imposed a reduction of 50 % of the Andean heights as a whole, but the uplift of the Andes was diachronous and not uniform (Boschman, 2021). In this sense, the imposed scenario could have been more realistic by imposing a western flank with closer-to-modern altitudes and an eastern flank with lesser altitudes (~50 % of modern values), as estimated by around 5–10 million years ago (Garzione et al., 2017). On the other hand, other experiments have performed more spatially-uniform experiments by prescribing the whole Andean cordillera to the same reductions (e.g., Insel et al., 2010; Poulsen et al., 2010), finding an abrupt increase in precipitation at the eastern flank when the Andean elevations reach about 70 % of modern elevations.

Furthermore, we do not account for such past conditions in our lateral boundary conditions, as they are based on DJF 2012–13 conditions in ERA5 reanalysis. The advantage of the present setup is its relative simplicity, isolating the impact of local topographic features directly upon atmospheric circulation leading to rainfall over the Quincemil hotspot. The results reveal significant changes in its extension and intensity due to the moisture flux intensity and direction changes by atmospheric adjustments to the removed topographies. Nevertheless, a more sophisticated setup is needed to consider the impacts of the aforementioned paleoclimatic and paleotectonic features in order to shed light on the origin of the Quincemil hotspot region and its implications on the evolution of landscape and biodiversity.

When we analyzed regional climate controls by the Fitzcarrald Arch and the Camisea mountain, we found an increase in rainfall to the east of a modern wetland known as Llanos de Moxos (Fig. 10 and Fig. 1a). This is associated with the cyclonic phase of a wave-like anomaly in IVT (Fig. 11). We tried to investigate the potential impacts of local topographic structures on regional climate by applying a technique known as two-way-nesting (TWN). This technique was previously applied to investigate the two-way interactions between a nested domain and its parent domain in regional scale impacts on global climate (e.g., Junquas et al., 2016; Lorenz and Jacob, 2005). However, besides reductions of biases in the area of the child domain, no significant results were found

(see Figs. S2 and S3 in the Supplementary Material). Yet, both the results from the d01 domain and the TWN experiments aim to solely assess the impact of local topography around Quincemil on regional atmospheric circulation, and do not consider other climate factors, as stated in the previous paragraph. In particular, the region downwind affected by the removal of Fitzcarrald Arch and Camisea mountain is located around the hypothesized southern tip of the Miocene megawetland with marine influence, connected to the Caribbean Sea and known as Pebas System (Hoorn et al., 2010). These land cover changes can potentially modify the distribution of atmospheric moisture and associated mesoscale vertical circulations, but are not taken into consideration in this study.

Two limitations arise due to the setup of the NLC50A experiment. First, it produces a discontinuity in the southern boundary (23°S) between the WRF d01 solutions in half-reduced Andes and the ERA5 boundary conditions based on "complete" topography. While this might introduce a potential source of numerical error, the dominance of moisture flux from equatorial latitudes over the model's domain (Fig. 11a) could effectively mitigate the propagation of errors associated to the southernmost boundary. Lastly, this setup does not allow us to explore the impacts of the Andean cordillera on global atmospheric dynamics. While we focused only on the atmospheric dynamics associated to the Quincemil hotspot rainfall with a high-resolution numerical atmospheric model, we refer the reader to Junquas et al. (2016) for numerical experiments on the influence of the Andes on regional and global scales circulation.

These results also motivate the consideration of the representation of the documented mechanisms in the location and intensity of the Quincemil hotspot in climate models and future climate projections. The coarse grid size of climate models used in the production of climate change simulations leads to considerable smoothing of the model topography. Such issues might pose biased atmospheric mechanisms around the Quincemil hotspot region, which could result in incorrect extensions and intensities of rainfall hotspots in the Andes-Amazon transition region (Gutierrez et al., 2024). Such misrepresentations can also be extended to future climate projections, in particular to those in response to increased greenhouse gas concentrations and deforestation. Recent studies using global and regional climate models showed that both perturbations can lead to energetic and moisture flux changes, both at local and regional scales (e.g., Agudelo et al., 2023; Arias et al., 2023; Sierra et al., 2022, 2023). Nevertheless, model biases in the representation of local atmospheric processes around Quincemil might constrain these results at the local scale.

CRediT authorship contribution statement

Ricardo A. Gutierrez-Villarreal: Writing – review & editing, Writing – original draft, Visualization, Validation, Software, Methodology, Investigation, Formal analysis, Data curation, Conceptualization. **Clémentine Junquas:** Writing – review & editing, Validation, Supervision, Resources, Project administration, Methodology, Formal analysis, Conceptualization. **Jhan-Carlo Espinoza:** Writing – review & editing, Validation, Supervision, Methodology, Funding acquisition, Conceptualization. **Patrice Baby:** Writing – review & editing, Validation, Methodology, Conceptualization. **Elisa Armijos:** Writing – review & editing, Project administration, Funding acquisition, Conceptualization.

Declaration of competing interest

The authors declare that they have no known competing financial interests or personal relationships that could have appeared to influence the work reported in this paper.

Acknowledgements

We would like to show our gratitude to Pierre Sepulchre (LSCE/IPSL, France), whose insights and expertise greatly helped to improve our research. We are also grateful to Alan Llacza (SENAMHI, Perú) for the availability of rain gauge data around the Quincemil hotspot. This research was funded by the Subdirección de Ciencias de la Atmósfera e Hidrósfera - Instituto Geofísico del Perú (SCAH-IGP), the No. 77-2021-FONDECYT/BM Project, the French AMANECER-MOPGA project funded by ANR and IRD (Ref. ANR-18-MPGA-0008) and the Water Cycle and Climate Change project (CECC; IRD/AFD). Most of the computations presented in this paper were performed using the GRICAD infrastructure (https://gricad.univ-grenoble-alpes.fr), which is supported by Grenoble research communities.

Appendix A. Supplementary data

Supplementary data to this article can be found online at https://doi.org/10.1016/j.atmosres.2025.108068.

Data availability

Data will be made available on request.

References

Agudelo, J., Espinoza, J.C., Junquas, C., Arias, P.A., Sierra, J.P., Olmo, M.E., 2023. Future projections of low-level atmospheric circulation patterns over south tropical South America: impacts on precipitation and Amazon dry season length. J. Geophys. Res. Atmos. 128 (22), e2023JD038658. https://doi.org/10.1029/2023JD038658.

Antonelli, A., Kissling, W.D., Flantua, S.G.A., Bermúdez, M.A., Mulch, A., Muellner-Riehl, A.N., Kreft, H., Linder, H.P., Badgley, C., Fjeldså, J., Fritz, S.A., Rahbek, C., Herman, F., Hooghiemstra, H., Hoorn, C., 2018. Geological and climatic influences on mountain biodiversity. Nat. Geosci. 11 (10), 10. https://doi.org/10.1038/s41561-018-0236-z.

Arias, P.A., Rendón, M.L., Martínez, J.A., Allan, R.P., 2023. Changes in atmospheric moisture transport over tropical South America: an analysis under a climate change scenario. Climate Dynam. 61 (11−12), 4949–4969. https://doi.org/10.1007/s00382-023-06833-4.

Armijos, E., Crave, A., Espinoza, J.C., Filizola, N., Espinoza-Villar, R., Ayes, Fonseca, P., Fraizy, P., Gutierrez, O., Vauchel, P., Camenen, B., Martinez, J.M., Santos, A.D., Santini, W., Cochonneau, G., Guyot, J.L., 2020. Rainfall control on Amazon sediment flux: Synthesis from 20 years of monitoring. Environmental Research Communications 2 (5), 051008. https://doi.org/10.1088/2515-7620/ab9003.

Athaydes, D., Dias, C.A.R., Gregorin, R., Perini, F.A., 2021. Evolution and biogeographic history of the Saguinus mystax group (Primates, Callithrichidae). Am. J. Primatol. 83 (2), e23226. https://doi.org/10.1002/ajp.23226.

Beveridge, C.F., Espinoza, J.-C., Athayde, S., Correa, S.B., Couto, T.B.A., Heilpern, S.A., Jenkins, C.N., Piland, N.C., Utsunomiya, R., Wongchuig, S., Anderson, E.P., 2024. The Andes-Amazon-Atlantic pathway: a foundational hydroclimate system for social-ecological system sustainability. Proc. Natl. Acad. Sci. U. S. A. 121 (22), e2306229121. https://doi.org/10.1073/pnas.2306229121.

Blackadar, A.K., 1957. Boundary Layer Wind Maxima and Their Significance for the Growth of Nocturnal Inversions. https://journals.ametsoc.org/view/journals/bams/38/5/1520-0477-38_5_283.xml.

Boschman, L.M., 2021. Andean mountain building since the Late Cretaceous: a paleoelevation reconstruction. Earth Sci. Rev. 220, 103640. https://doi.org/10.1016/j.earscirev.2021.103640.

Chavez, S.P., Takahashi, K., 2017. Orographic rainfall hot spots in the Andes-Amazon transition according to the TRMM precipitation radar and in situ data. J. Geophys. Res. Atmos. 122 (11), 5870–5882. https://doi.org/10.1002/2016JD026282.

Dominguez, F., Rasmussen, R., Liu, C., Ikeda, K., Prein, A., Varble, A., Arias, P.A., Bacmeister, J., Bettolli, M.L., Callaghan, P., Carvalho, L.M.V., Castro, C.L., Chen, F., Chug, D., Chun, K.P. (Sun), Dai, A., Danaila, L., Rocha, R.P.D., Nascimento, E.D.L., Schneider, T., 2023. Advancing South American water and climate science through multi-decadal convection-permitting modeling. Bull. Am. Meteorol. Soc. https://doi.org/10.1175/BAMS-D-22-0226.1.

Dudhia, J., 1989. Numerical study of convection observed during the winter monsoon experiment using a mesoscale two-dimensional model. J. Atmos. Sci. 46 (20), 3077–3107. https://doi.org/10.1175/1520-0469(1989)046<3077:NSOCOD>2.0.CO;2.

Espinoza, J.C., Chavez, S., Ronchail, J., Junquas, C., Takahashi, K., Lavado, W., 2015. Rainfall hotspots over the southern tropical Andes: spatial distribution, rainfall intensity, and relations with large-scale atmospheric circulation. Water Resour. Res. 51 (5), 3459–3475. https://doi.org/10.1002/2014WR016273.

Espinoza, J.C., Garreaud, R., Poveda, G., Arias, P.A., Molina-Carpio, J., Masiokas, M., Viale, M., Scaff, L., 2020. Hydroclimate of the Andes part I: main climatic features. Front. Earth Sci. 8, 64. https://doi.org/10.3389/feart.2020.00064.

Espurt, N., Baby, P., Brusset, S., Roddaz, M., Hermoza, W., Regard, V., Antoine, P.-O., Salas-Gismondi, R., Bolaños, R., 2007. How does the Nazca Ridge subduction influence the modern Amazonian foreland basin? Geology 35 (6), 515–518. https://doi.org/10.1130/G23237A.1.

Espurt, N., Baby, P., Brusset, S., Roddaz, M., Hermoza, W., Barbarand, J., 2009. The Nazca Ridge and Uplift of the Fitzcarrald Arch. In: Implications for Regional Geology in Northern South America. En Amazonia: Landscape and Species Evolution. John Wiley & Sons, Ltd., pp. 89–100. https://doi.org/10.1002/9781444306408.ch6

Figueroa, S.N., Satyamurty, P., Dias, P.L.D.S., 1995. Simulations of the Summer Circulation over the South American Region with an Eta Coordinate Model. J. Atmos. Sci. 52 (10), 1573–1584. https://doi.org/10.1175/1520-0469(1995)052<1573:SOTSCO>2.0.CO;2.

Flores-Rojas, J.L., Moya-Álvarez, A.S., Valdivia-Prado, J.M., Piñas-Laura, M., Kumar, S., Karam, H.A., Villalobos-Puma, E., Martínez-Castro, D., Silva, Y., 2021. On the dynamic mechanisms of intense rainfall events in the central Andes of Peru, Mantaro valley. Atmospheric Research 248, 105188. https://doi.org/10.1016/j.atmosres.2020.105188.

Garreaud, RenéD, 1999. Multiscale analysis of the summertime precipitation over the Central Andes. Mon. Weather Rev. 127 (5), 901–921. https://doi.org/10.1175/1520-0493(1999)127<0901:MAOTSP>2.0.CO;2.

Garreaud, R.D., 2009. The Andes climate and weather. Advances in Geosciences 22, 3–11, 4th EGU Alexander von Humboldt Conference "The Andes: Challenge for Geosciences" - 4th Alexander von Humboldt International Conference on The Andes: Challenge for Geosciences, Santiago de Chile, Chile, 24–28 November 2008. https://doi.org/10.5194/adgeo-22-3-2009.

Garzione, C.N., McQuarrie, N., Perez, N.D., Ehlers, T.A., Beck, S.L., Kar, N., Eichelberger, N., Chapman, A.D., Ward, K.M., Ducea, M.N., Lease, R.O., Poulsen, C. J., Wagner, L.S., Saylor, J.E., Zandt, G., Horton, B.K., 2017. Tectonic evolution of the Central Andean Plateau and implications for the growth of plateaus. Annu. Rev. Earth Planet. Sci. 45 (1), 529–559. https://doi.org/10.1146/annurev-earth-063016-020612.

Gomez-Rios, S., Zuluaga, M.D., Hoyos, C.D., 2023. Orographic controls over convection in an inter-andean valley in Northern South America. Mon. Weather Rev. 151 (1), 145–162. https://doi.org/10.1175/MWR-D-21-0231.1.

Gutierrez, R.A., Junquas, C., Armijos, E., Sörensson, A.A., Espinoza, J.-C., 2024. Performance of regional climate model precipitation simulations over the terrain-complex Andes-Amazon transition region. J. Geophys. Res. Atmos. 129 (1), e2023JD038618. https://doi.org/10.1029/2023JD038618.

Hersbach, H., Bell, B., Berrisford, P., Hirahara, S., Horányi, A., Muñoz-Sabater, J., Nicolas, J., Peubey, C., Radu, R., Schepers, D., Simmons, A., Soci, C., Abdalla, S., Abellan, X., Balsamo, G., Bechtold, P., Biavati, G., Bidlot, J., Bonavita, M., et al., 2020. The ERA5 global reanalysis. Q. J. R. Meteorol. Soc. 146 (730), 1999–2049. https://doi.org/10.1002/qj.3803.

Hong, S.-Y., Noh, Y., Dudhia, J., 2006. A new vertical diffusion package with an explicit treatment of entrainment processes. Mon. Weather Rev. 134 (9), 2318–2341. https://doi.org/10.1175/MWR3199.1.

Hoorn, C., Wesselingh, F.P., ter Steege, H., Bermudez, M.A., Mora, A., Sevink, J., Sanmartín, I., Sanchez-Meseguer, A., Anderson, C.L., Figueiredo, J.P., Jaramillo, C., Riff, D., Negri, F.R., Hooghiemstra, H., Lundberg, J., Stadler, T., Särkinen, T., Antonelli, A., 2010. Amazonia through time: Andean uplift, climate change, landscape evolution, and biodiversity. Science 330 (6006), 927–931. https://doi.org/10.1126/science.1194585.

Hu, X.-M., Huang, Y., Xue, M., Martin, E., Hong, Y., Chen, M., Novoa, H.M., McPherson, R., Perez, A., Morales, I.Y., Luna, A.J.F., 2023. Effects of lower troposphere vertical mixing on simulated clouds and precipitation over the Amazon during the wet season. J. Geophys. Res. Atmos. 128 (12), e2023JD038553. https://doi.org/10.1029/2023JD038553.

Huang, Y., Xue, M., Hu, X.-M., Martin, E., Novoa, H.M., McPherson, R.A., Perez, A., Morales, I.Y., 2023. Convection-permitting simulations of precipitation over the Peruvian Central Andes: strong sensitivity to planetary boundary layer parameterization. J. Hydrometeorol. 24 (11), 1969–1990. https://doi.org/10.1175/JHM-D-22-0173.1.

Huerta, A., Lavado-Casimiro, W., Felipe-Obando, O., 2022. High-resolution gridded hourly precipitation dataset for Peru (PISCOp_h). Data Brief 45, 108570. https://doi.org/10.1016/j.dib.2022.108570.

Insel, N., Poulsen, C.J., Ehlers, T.A., 2010. Influence of the Andes Mountains on South American moisture transport, convection, and precipitation. Climate Dynam. 35 (7–8), 1477–1492. https://doi.org/10.1007/s00382-009-0637-1.

Joyce, R.J., Janowiak, J.E., Arkin, P.A., Xie, P., 2004. CMORPH: a method that produces global precipitation estimates from passive microwave and infrared data at high spatial and temporal resolution. J. Hydrometeorol. 5 (3), 487–503. https://doi.org/10.1175/1525-7541(2004)005<0487:CAMTPG>2.0.CO;2.

Junquas, C., Li, L., Vera, C.S., Le Treut, H., Takahashi, K., 2016. Influence of South America orography on summertime precipitation in Southeastern South America. Climate Dynam. 46 (11–12), 3941–3963. https://doi.org/10.1007/s00382-015-2814-8.

Junquas, C., Takahashi, K., Condom, T., Espinoza, J.-C., Chavez, S., Sicart, J.-E., Lebel, T., 2018. Understanding the influence of orography on the precipitation diurnal cycle and the associated atmospheric processes in the central Andes. Climate Dynam. 50 (11–12), 3995–4017. https://doi.org/10.1007/s00382-017-3858-8.

Junquas, C., Heredia, M.B., Condom, T., Ruiz-Hernández, J.C., Campozano, L., Dudhia, J., Espinoza, J.C., Menegoz, M., Rabatel, A., Sicart, J.E., 2022. Regional climate modeling of the diurnal cycle of precipitation and associated atmospheric circulation patterns over an Andean glacier region (Antisana, Ecuador). Climate Dynam. 58 (11–12), 3075–3104. https://doi.org/10.1007/s00382-021-06079-y.

Junquas, C., Martinez, J.A., Bozkurt, D., Viale, M., Fita, L., Trachte, K., Campozano, L., Arias, P.A., Boisier, J.P., Condom, T., Goubanova, K., Pabón-Caicedo, J.D., Poveda, G., Solman, S.A., Sörensson, A.A., Espinoza, J.C., 2024. Recent progress in atmospheric modeling over the Andes – part II: projected changes and modeling challenges. Front. Earth Sci. 12, 1427837. https://doi.org/10.3389/feart.2024.1427837.

Kendon, E.J., Prein, A.F., Senior, C.A., Stirling, A., 2021. Challenges and outlook for convection-permitting climate modelling. Philos. Trans. R. Soc. A Math. Phys. Eng. Sci. 379 (2195), 20190547. https://doi.org/10.1098/rsta.2019.0547.

Lenters, J.D., Cook, K.H., 1997. On the origin of the Bolivian high and related circulation features of the South American climate. J. Atmos. Sci. 54 (5), 656–678. https://doi.org/10.1175/1520-0469(1997)054<0656:OTOOTB>2.0.CO;2.

Li, Z.X., Le Treut, H., 1999. Transient behavior of the meridional moisture transport across South America and its relation to atmospheric circulation patterns. Geophys. Res. Lett. 26 (10), 1409–1412. https://doi.org/10.1029/1999GL900274.

Lorenz, P., Jacob, D., 2005. Influence of regional scale information on the global circulation: a two-way nesting climate simulation. Geophys. Res. Lett. 32 (18). https://doi.org/10.1029/2005GL023351.

Marengo, J.A., Soares, W.R., Saulo, C., Nicolini, M., 2004. Climatology of the low-level jet east of the andes as derived from the NCEP–NCAR reanalyses: characteristics and temporal variability. J. Climate 17 (12), 2261–2280. https://doi.org/10.1175/1520-0442(2004)017<2261:COTLJE>2.0.CO;2.

Martinez, J.A., Arias, P.A., Junquas, C., Espinoza, J.C., Condom, T., Dominguez, F., Morales, J.S., 2022. The orinoco low-level jet and the cross-equatorial moisture transport over tropical South America: lessons from seasonal WRF simulations. J. Geophys. Res. Atmos. 127 (3), e2021JD035603.

Martinez, J.A., Junquas, C., Bozkurt, D., Viale, M., Fita, L., Trachte, K., Campozano, L., Arias, P.A., Boisier, J.P., Condom, T., Goubanova, K., Pabón-Caicedo, J.D., Poveda, G., Solman, S.A., Sörensson, A.A., Espinoza, J.C., 2024. Recent progress in atmospheric modeling over the Andes – part I: review of atmospheric processes. Front. Earth Sci. 12, 1427783. https://doi.org/10.3389/feart.2024.1427783.

Mlawer, E.J., Taubman, S.J., Brown, P.D., Iacono, M.J., Clough, S.A., 1997. Radiative transfer for inhomogeneous atmospheres: RRTM, a validated correlated-k model for the longwave. J. Geophys. Res. Atmos. 102 (D14), 16663–16682. https://doi.org/10.1029/97JD00237.

Montini, T.L., Jones, C., Carvalho, L.M.V., 2019. The South American low-level jet: a new climatology, variability, and changes. J. Geophys. Res. Atmos. 124 (3), 1200–1218. https://doi.org/10.1029/2018JD029634.

Morrison, H., Thompson, G., Tatarskii, V., 2009. Impact of cloud microphysics on the development of trailing stratiform precipitation in a simulated squall line: comparison of one- and two-moment schemes. Mon. Weather Rev. 137 (3), 991–1007. https://doi.org/10.1175/2008MWR2556.1.

Mourre, L., Condom, T., Junquas, C., Lebel, T., E. Sicart, J., Figueroa, R., Cochachin, A., 2016. Spatio-temporal assessment of WRF, TRMM and in situ precipitation data in a tropical mountain environment (Cordillera Blanca, Peru). Hydrol. Earth Syst. Sci. 20 (1), 125–141. https://doi.org/10.5194/hess-20-125-2016.

Mulholland, J.P., Nesbitt, S.W., Trapp, R.J., 2019. A case study of terrain influences on upscale convective growth of a supercell. Mon. Weather Rev. 147 (12), 4305–4324. https://doi.org/10.1175/MWR-D-19-0099.1.

Nakanishi, M., Niino, H., 2009. Development of an improved turbulence closure model for the atmospheric boundary layer. Journal of the Meteorological Society of Japan. Ser. II 87 (5), 895–912. https://doi.org/10.2151/jmsj.87.895.

Negri, A.J., Bell, T.L., Xu, L., 2002. Sampling of the diurnal cycle of precipitation using TRMM. J. Atmos. Oceanic Tech. 19 (9), 1333–1344. https://doi.org/10.1175/1520-0426(2002)019<1333:SOTDCO>2.0.CO;2.

Paulson, C.A., 1970. The mathematical representation of wind speed and temperature profiles in the unstable atmospheric surface layer. Journal of Applied Meteorology and Climatology 9 (6), 857–861. https://doi.org/10.1175/1520-0450(1970)009<0857:TMROWS>2.0.CO;2.

Pleim, J.E., 2007. A combined local and nonlocal closure model for the atmospheric boundary layer. Part I: model description and testing. J. Appl. Meteorol. Climatol. 46 (9), 1383–1395. https://doi.org/10.1175/JAM2539.1.

Poulsen, C.J., Ehlers, T.A., Insel, N., 2010. Onset of convective rainfall during gradual Late Miocene rise of the Central Andes. Science 328 (5977), 490–493. https://doi.org/10.1126/science.1185078.

Rasmussen, K.L., Houze, R.A., 2016. Convective initiation near the Andes in subtropical South America. Mon. Weather Rev. 144 (6), 2351–2374. https://doi.org/10.1175/MWR-D-15-0058.1.

Regard, V., Lagnous, R., Espurt, N., Darrozes, J., Baby, P., Roddaz, M., Calderon, Y., Hermoza, W., 2009. Geomorphic evidence for recent uplift of the Fitzcarrald Arch (Peru): a response to the Nazca Ridge subduction. Geomorphology 107 (3), 107–117. https://doi.org/10.1016/j.geomorph.2008.12.003.

Romatschke, U., Houze, R.A., 2010. Extreme summer convection in South America. J. Climate 23 (14), 3761–3791. https://doi.org/10.1175/2010JCLI3465.1.

Roncal, J., Couderc, M., Baby, P., Kahn, F., Millán, B., Meerow, A.W., Pintaud, J.-C., 2015. Palm diversification in two geologically contrasting regions of western Amazonia. J. Biogeogr. 42 (8), 1503–1513. https://doi.org/10.1111/jbi.12518.

Rosales, A.G., Junquas, C., da Rocha, R.P., Condom, T., Espinoza, J.-C., 2022. Valley–mountain circulation associated with the diurnal cycle of precipitation in the tropical Andes (Santa River Basin, Peru). Atmosphere 13 (2), 344.

Sacek, V., Mutz, S.G., Bicudo, T.C., de Almeida, R.P., Ehlers, T.A., 2023. The Amazon paleoenvironment resulted from geodynamic, climate, and sea-level interactions. Earth Planet. Sci. Lett. 605, 118033. https://doi.org/10.1016/j.epsl.2023.118033.

Saurral, R.I., Camilloni, I.A., Ambrizzi, T., 2015. Links between topography, moisture fluxes pathways and precipitation over South America. Climate Dynam. 45 (3–4), 777–789. https://doi.org/10.1007/s00382-014-2309-z.

Sepulchre, P., Sloan, L.C., Fluteau, F., 2009. Modelling the response of Amazonian climate to the uplift of the Andean Mountain range. In: En Amazonia: Landscape and Species Evolution. John Wiley & Sons, Ltd., pp. 211–222. https://doi.org/10.1002/9781444306408.ch13

Sierra, J.P., Junquas, C., Espinoza, J.C., Segura, H., Condom, T., Andrade, M., Molina-Carpio, J., Ticona, L., Mardoñez, V., Blacutt, L., 2022. Deforestation impacts on Amazon-Andes hydroclimatic connectivity. Climate Dynam. 58 (9), 2609–2636.

Sierra, J.P., Espinoza, J.-C., Junquas, C., Wongchuig, S., Polcher, J., Moron, V., Fita, L., Arias, P.A., Schrapffer, A., Pennel, R., 2023. Impacts of land-surface heterogeneities and Amazonian deforestation on the wet season onset in southern Amazon. Climate Dynam. 61 (9), 4867–4898. https://doi.org/10.1007/s00382-023-06835-2.

Skamarock, C., Klemp, B., Dudhia, J., Gill, O., Liu, Z., Berner, J., Wang, W., Powers, G., Duda, G., Barker, D., Huang, X., 2021. A Description of the Advanced Research WRF Model Version 4.3. https://doi.org/10.5065/1dfh-6p97.

Tejada-Lara, J.V., Salas-Gismondi, R., Pujos, F., Baby, P., Benammi, M., Brusset, S., De Franceschi, D., Espurt, N., Urbina, M., Antoine, P.-O., 2015. Life in proto-Amazonia: middle Miocene mammals from the Fitzcarrald Arch (Peruvian Amazonia). Palaeontology 58 (2), 341–378. https://doi.org/10.1111/pala.12147.

Trachte, K., Nauss, T., Bendix, J., 2009. The impact of different terrain configurations on the formation and dynamics of Katabatic flows: idealised case studies. Bound.-Lay. Meteorol. 134, 307–325. https://doi.org/10.1007/s10546-009-9445-8.

Trachte, K., Rollenbeck, R., Bendix, J., 2010. Nocturnal convective cloud formation under clear-sky conditions at the eastern Andes of south Ecuador. J. Geophys. Res. Atmos. 115 (D24). https://doi.org/10.1029/2010JD014146.

TRMM Precipitation Radar Team, 2011. Tropical rainfall measuring mission (TRMM) precipitation radar algorithm: Instruction manual for version 7. Available at http://www.eorc.jaxa.jp/TRMM/documents/PR_algorithm_product_information/pr_manual/PR_Instruction_Manual_V7_L1.pdf.

Vera, C., Baez, J., Douglas, M., Emmanuel, C.B., Marengo, J., Meitin, J., Nicolini, M., Nogues-Paegle, J., Paegle, J., Penalba, O., Salio, P., Saulo, C., Dias, M.A.S., Dias, P.S., Zipser, E., 2006a. The South American low-level jet experiment. Bull. Am. Meteorol. Soc. 87 (1), 63–78. https://doi.org/10.1175/BAMS-87-1-63.

Vera, C., Higgins, W., Amador, J., Ambrizzi, T., Garreaud, R., Gochis, D., Gutzler, D., Lettenmaier, D., Marengo, J., Mechoso, C.R., Nogues-Paegle, J., Dias, P.L.S., Zhang, C., 2006b. Toward a unified view of the American monsoon systems. J. Climate 19 (20), 4977–5000. https://doi.org/10.1175/JCLI3896.1.

Xiang, R., Steger, C.R., Li, S., Pellissier, L., Sørland, S.L., Willett, S.D., Schär, C., 2024. Assessing the regional climate response to different Hengduan mountains geometries with a high-resolution regional climate model. J. Geophys. Res. Atmos. 129 (6), e2023JD040208. https://doi.org/10.1029/2023JD040208.

Yabra, M.S., Nicolini, M., Borque, P., Skabar, Y.G., Salio, P., 2022. Observational study of the South American low-level jet during the SALLJEX. Int. J. Climatol. 42 (16), 9676–9696. https://doi.org/10.1002/joc.7857.

Yang, Z.-L., Niu, G.-Y., Mitchell, K.E., Chen, F., Ek, M.B., Barlage, M., Longuevergne, L., Manning, K., Niyogi, D., Tewari, M., Xia, Y., 2011. The community Noah land surface model with multiparameterization options (Noah-MP): 2. Evaluation over global river basins. Journal of Geophysical Research: Atmospheres 116 (D12). https://doi.org/10.1029/2010JD015140.

Zhang, C., Wang, Y., 2017. Projected future changes of tropical cyclone activity over the Western North and South Pacific in a 20-km-Mesh regional climate model. J. Climate 30 (15), 5923–5941. https://doi.org/10.1175/JCLI-D-16-0597.1.

Zubieta, R., Saavedra, M., Espinoza, J.C., Ronchail, J., Sulca, J., Drapeau, G., Martin-Vide, J., 2019. Assessing precipitation concentration in the Amazon basin from different satellite-based data sets. Int. J. Climatol. 39 (7), 3171–3187. https://doi.org/10.1002/joc.6009.